Experimental evaluation of rolling contact fatigue in railroad wheels

Elsevier Editorial System(tm) for
International Journal of Fatigue
Manuscript Draft

Manuscript Number: IJFATIGUE-D-16-00146R1

Title: EXPERIMENTAL EVALUATION OF ROLLING CONTACT FATIGUE IN RAILROAD WHEELS

Article Type: Original Research Paper

Keywords: rolling contact fatigue; crack propagation; fatigue; rail vehicles; railway engineering.

Corresponding Author: Dr. Pasquale Gallo, Ph.D.

Corresponding Author's Institution: Aalto University

First Author: Cesar A Sciammarella

Order of Authors: Cesar A Sciammarella; R J Chen; Pasquale Gallo; Filippo Berto; Luciano Lamberti

Manuscript Region of Origin: Europe

Response to Reviewers: Reviewer's comments have been provided in a separate file.

Aalto University
School of Engineering

To Professor M.N. James,
Editor of International Journal of Fatigue
27 May 2016

Dear Prof. James,

On behalf of my co-authors, I submit the revised manuscript entitled: **EXPERIMENTAL EVALUATION OF ROLLING CONTACT FATIGUE IN RAILROAD WHEELS (**C.A. Sciammarella, R.J.S. Chen, P. Gallo, F. Berto, L. Lamberti) to your Journal.

We apologize once again for the delay but this work involved several people and a huge amount of work made in the last years. For this reason the procedure of the revision has been very difficult for us. I want to add some minor comments:

-we tried to answer in the best possible way to the reviewers and we re-wrote almost all the manuscript. All the major modifications have been underlined in the marked manuscript.

-both reviewers argued that the mechanical properties of the tested material are missing, unfortunately the company cannot share detailed information on this point and even if we tried to get those information we did not success. We hope the reviewers will understand our position.

Thank you so much for your time and consideration,

we look forward to hearing from you once you take a decision.

Sincerely yours,

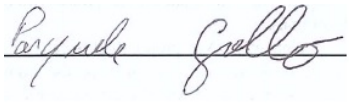

Pasquale Gallo

Aalto University
Department of Mechanical Engineering, Marine Technology
Puumiehenkuja 5A,
02150 Espoo, Finland

RESPONSE TO REVIEWER'S COMMENTS

The authors are really grateful to the Reviewers for their effort in reviewing the present manuscript. The revision activity takes time and effort, and the authors really appreciate the detailed comments presented by the reviewers.
For these reasons, all the raised points have been accurately took into account in order to improve the overall quality of the work. Below you can find answers point by point. All the changes have been highlighted in the "marked manuscript".

Reviewer #1

…However, the discussion of the results in my opinion is very unsatisfactory: it appears confusing, unclear, rather qualitative and unrelated to the experimental results of the authors. They made some qualitative comparisons with the results obtained by other authors in very different conditions, not authorising some deductions they inferred. Furthermore, some concluding remarks (even reported in the highlights) are not linked with the previous discussion. For this reason, I think that a "normal" revision process is not sufficient: the authors should rewrite the article, highlighting more specifically what can be obtained from their experimental results, enforcing their conclusion by a quantitative elaboration.

The authors spent much effort in the revision of the present manuscript. It has been totally revised and rewritten extensively. We also addressed all the points raised by the Reviewers and comments/details have been added to the manuscript.

- Page 15, rows 16-33: what the Authors mean for "adhesion zone" and "slip zone"? I guess that in the adhesion zone there is contact without relative sliding, whereas in the slip region there is contact with relative sliding. If this is correct, how can be affirmed that the adhesion zone is reduced even by the normal forces? (rows 30-31).

The adhesion zone and the slip zone are standard terms utilized in the study of the rolling contact and can be found in any textbook. This is a classical problem that has been dealt with in the literature since it is a fundamental concept to understand the interaction of two surfaces. However, the text has been modified to remove any ambiguity (pag. 14 of revised manuscript) and an extensive discussion on adhesion and slip zones has been included in pp. 14-15, Section 5.2 of revised manuscript.

- Page 15, rows 34-40: in Fig. 17 two maps of residual stresses are introduced: nothing is stated about who and how obtained these maps, in what condition, etc.

The figure (renumbered as Figure 18 in the revised article) refers to a previous study carried out by the first author (C.A. Sciammarella: "Friction Creep and Wear Studies Between Steel Wheels and Rails." U.S. Department of Transportation, Federal Administration Office of Development and Reseach, Report N FRA-OR and D-76-271, July 1976). This has been explained in the revised article by adding the paragraph "*As the contact becomes dynamic... size of the adhesion region and the slip zone.*" to Section 5.2 (pag. 14-15 of revised manuscript).

- Page 15, rows 42-53: in Fig. 18 a photoelastic pattern of a plate under uniform load is shown, and a scaled experimental crack is superposed in order to show the similitude of its path with the photoelastic fringes. This comparison is improper, both because the loading condition is different and because the experimental crack developed within a heavy plastic

stress-strain domain, as the authors themselves stated. This comparison does not show anything relevant.

The authors respectfully disagree with the Reviewer and do believe that Figure 18 (renumbered as Figure 20 in the revised article) is quite relevant. Indeed, there are several mechanisms in the damage produced by the rolling contact of two surfaces. There is a surface damage caused by the presence of roughness that through high cycle fatigue leads to the scaling separation of material shown in Figure 22. A separate mechanism of damage is caused by the fatigue caused by the bulk stress field that caused the cracks shown in Figures 1 and 12. This process is a classical fatigue crack propagation under a 3-D state of stresses. The Reviewer can look at a recent experimental verification on this subject: C.A. Sciammarella et al. *Investigation on fracture behaviour of turbine blades under self-exciting modes*. Strain, 47 Issue Supplement S1, pp. e113-e129, 2011. The fracture takes place along the isostatics of the stress field that are lines of maximum damage. In this case the lines of maximum damage are the lines of maximum shear. This explain the similitude of shape between the observed shear strains in the photoelastic pattern and the crack trajectory observed in the present experiments. The shear stresses correspond to contact stresses with friction and are shown as additional information to help the reader to visualize the stress field that prevails in the contact problem.
The above discussion has been added into Section 5.2, pag. 16 of the revised article.

- **Page 15, rows 55-61: the relationship between the results shown in Fig. 19 and the authors' results again is unclear. The curves refer to a very different stress-state condition with respect to the experiments (elastic regime, different material); furthermore, they show very well known results. In Figure 19c an "experimental" curve appears, but nothing is written about it.**

The authors respectfully disagree with the Reviewer on the lack of relationship between Fig. 19 (renumbered as Fig. 17 in the revised article) and the present results. However, the section is completely rewritten to improve readability (pp. 14-15 of the revised article).
Experimental results shown in Figures 19 and 20 (respectively renumbered as Figures 17 and 19 in the revised article) come from an application of moiré to analyze contact stresses under normal load and friction (the Reviewer can look at the references cited in the article), a similar condition to the present experiments, although in the static regime. Figure 19 (Figure 17 of revised article) illustrates the concept of adhesion zone and slide zone in static contact. The study corresponds to a 3-D distribution of stresses that due to the symmetry can be studied in a 2-D plane. It can be seen the difference between the classical Hertz solution normal contact stresses and the actual distribution measured experimentally when friction is present. The effect of tangential stress and the transition from adhesion zone (tensile strain) to the slip zone (compressive strain) also are clarified. Figure 20 (Figure 19 of revised article) presents additional experiments done on the contact problem. Again using the moiré method the displacement field in the contact zone of a cylinder in rolling on a surface is analyzed. Figure 20 (i.e. Figure 19 of revised article) is the equivalent of plotting the strain ε_{xx} of Figure 19 (Figure 17 of revised article) together with the curves already shown in Figure 20 (Figure 19 of revised article). It shows that in rolling contact, the attack zone host high tensile stresses that are the source of the bulk cracks.

- **Page 16, rows 1-13: in Figure 20 an improper comparison is made, as the two curves were obtained in different conditions. Nothing is stated about the way these curves were obtained; the x-axis refers to an undefined "normalised position". What does it mean that the "actual measured strains are scaled to make the visual comparison clearer"? Furthermore, I just cannot see the "qualitative agreement" between the two curves.**

- Page 16, rows 13-33: again, it is not clear what the authors mean as adhesion zone, and why this is limited by the points where <epsilon>xx is equal to zero (what is the x-direction?) Furthermore, the relationship between the stress history of a point in the rolling solid and the subsequent statement about the layered structure of the damaged material is obscure.

The preceding answer clarifies the question made by the Reviewer. The normalization position is very simple to understand. Since dimensions of the major axis of contact ellipse depend on the load and materials, the position of points is normalized by making the half axis equal 1. This is remarked in Section 5.2, pag. 15 of the revised article.

- Page 16 row 34 to page 17 row 36: in this paragraph the authors try to quantify the crack propagation rate in their experiments, but a qualitative discussion on crack propagation models follows, unrelated to their findings. Furthermore, the equations they recall are obtained for a linear elastic fracture mechanics context, very far from the condition experienced by the tested wheel materials where heavy plasticisation occurs.

We respectfully disagree with the Reviewer for the following reasons. There is a very important aspect of this question that needs clarifying. One is dealing with a fatigue case not a static loading case, one should be very cautious at using the idea of plasticity. Plasticity itself is a dynamic phenomenon that implies the motion of dislocations, this process implies the propagation of dislocations in waves, motion that is triggered by the loading process (see the recent paper C.A. Sciammarella and L. Lamberti, Merging experimental evidence and Molecular Dynamics theory to develop efficient models of solids fracture, 2016 SEM Conference on Experimental and Applied Mechanics). The material in the initial condition is elastic and as it is being loaded by the contact forces follows a stress-strain relation corresponding to a 3-D stress condition, and as a consequence of this condition at a given level dislocations are no longer stable and begin to propagate in a plastic wave that increases the damage of the material by coalescence of the dislocations within the volume. But since at a certain instant of time the load is reduced the material returns to the elastic state. This cycle repeats itself until in the damage zone reaches a level that coalescence of dislocations creates an actual crack that ultimately will lead to the fracture if the void created is big enough to generate the instability of the whole structure. The problem is very complex but it is possible on the basis of existing knowledge to make inferences concerning this process in a statistical sense.
This discussion has been added into Section 5.2, pag. 17 of revised article. The authors are really grateful to the Reviewer for the possibility to open the interesting discussion presented above.

-Even if the Authors applied water in the final phase of their experiments, nothing but a generic statement is said about this in the discussion, although water penetration into the cracks is a key factor for their propagation. Did the authors observe anything relevant in their experiments when they added water to contact?

The adding of water created pitting, that is the separation of chunks of material.

- Concluding remarks: these should be almost totally revised given the comments above; furthermore, in the last rows the Authors state that all propagation modes will be activated: this point is never discussed nor proven throughout the paper, and it cannot be "suddently" introduced into the conclusions and into the highlights.

The whole paper, not only the conclusion, has been totally revised. Please see the marked manuscript.

In addition to these comments, I add some minor ones:

- in Fig. 2 the number 3 is missing; furthermore, all numbers from 8 to 13 are missing in the legend.

The Reviewer is right. The number 3 (corresponding to the large wheel) has now been added. Moreover, the legend has been updated with the missing number. We believe that some errors occurred in the Word-PDF conversion.

- The material properties (commercial name or standard, chemical composition, mechanical properties) should be specified, in order to respect the principle that the reader has to be in condition of experimentally verifying the results.

We agree with the statement made by the Reviewer. However, we received the material from manufacturers of wheels that participated in the project, they did not provide further information on the difference of the materials (proprietary information). This is remarked in the revised article. We have tried to retrieve more information but, unfortunately we did not get a positive answer from the manufactures for the reasons above.

- Page 11, row 29: the statement "assumed a value of <mu>=0.2 to run the tests" is unclear.

This point has been also raised by Reviewer 2 and it has been clarified in the manuscript (see final part of Section 3.3). In detail: a relationship within the strain-gauge bridge and the friction coefficient was determined. In this way we are able to determine for each value of the coefficient, the corresponding value of the strain indicator and vice versa. For this reason, the desired friction coefficient has been assumed/imposed a priori, that is 0.2. The corresponding value of the strain is 272.5 με. In other words, if during the test the strain indicator reports 272.5 με, it means that with good approximation the friction coefficient is 0.2. For this reason, during experimental testing, we checked the strain indicator and assure that the value was as close as possible to 272.5 με in order to obtain the desired friction coefficient. The variation on the coefficient due to this indirect measurement has also been quantified in 0.7%.

- Everywhere: "load cycles" is preferable to "fatigue cycles"

All the figures and manuscript have been checked and updated. Thank you for the suggestion.

- Figure 10: in the ordinate axis units are missing

The rate of change of number of cracks with wear is a number divided by a mass, i.e. 1/mg. This is indicated in the article.

- Markers able to give the dimensional scale should be added to all micrographs.

The caption of the figures are provided by information of the magnification, when necessary. Scales can be derived from the average crack sizes reported in the article. All the other

micrographs are qualitative, in order to show the effect of the experimental test and the phenomenon involved.

Reviewer #2

1.Introduction

The authors review in detail the research progress about the RCF and wear in the wheel-rail contact. Some description should be simplified and reviewed. For example, Page 3, L7~24, Page 4, L18~35. The introduction it too long and should be rewritten and compressed.

The Introduction has been rewritten and shortened. Only the main results of the cited works have been left and the authors mainly focused on the lines suggested by the reviewer. All the changes have been highlighted in the marked manuscript.

- There is a competitive relationship between rolling contact fatigue damage and wear. The corresponding description should refer the literature (Wear 267 (2009) 540-544 and Engineering Fracture Mechanics 72 (2005) 287-308).

The suggested references have been added. The authors are really grateful to the Reviewer for the suggestions. See marked manuscript, Ref. (13) and Ref. (14).

2. Apparatus and experimental details

Some experimental parameters should be added and given some detailed description.

The paper has been accurately rewritten in every sections, accordingly also to the #Rev.1. Details and comments have been added when necessary.

- What is the number in Fig.2, such as 8~12?

Number from 8-12 have been now added to the legend. Thank you for the suggestion.

- Some information about six wheel materials should be given, for material properties including Chemical composition and mechanical properties of rail and wheel materials.

We received the material from manufacturers of wheels that participated in the project, they did not provide further information on the difference of the materials (proprietary information). This is remarked in the revised article. We have tried to retrieve more information but, unfortunately we did not get a positive answer from the manufactures for the reasons above.

- How to machine the wheel and rail specimens before testing? If from the wheel tread and rail head, how to cut? If not, how to ensure the microstructure of wheel and rail rollers compared with the real wheel/rail materials.

Materials and specimens were provided by manufacturers as the representative elements that they use in the manufacture of the corresponding parts. This is remarked in the revised article. The company cannot share more information due to industrial secrets, despite the fact that in the last weeks we tried to get a positive answer. We hope that the Reviewer will understand our position.

- The experiments should be carried out under the water condition. How much is the water flow? How to add during the experiment? If the experiments is carried out for the whole time under the water condition? I think that the surface crack is difficult to form and grow. So, the experimental condition should be described in detail.

The water test was conducted on wheels that have already been cracked. In the actual wheels and rails the presence of liquids influences the already cracked wheels; the liquid is an additional factor that adds a load to the existing crack. This is clarified in Section 2.3, pag. 8 of the revised article.

- The friction coefficient is 0.2. How to measure during the experiment?

Evaluation of the friction coefficient is a really important aspect in experimental testing. For this reason, we devoted the paragraph 3.3 to this matter. In detail, after calibration, the friction coefficient was determined through indirect measurement during the test as a function of the reading of the strain-gage bridge. Assuming a determined desired value of the coefficient a priori, that is 0.2, returns a determined value of the strain indicator, that is 272.5 με.
During the experimental testing, the value reported by the strain indicator has been checked to be as much close as possible to the value of 272.5 με, implying a value of the friction coefficient close to 0.2. The variation of the measure has been also quantified in a 0.7% variation of the friction coefficient.
In other words: the friction coefficient value has been imposed a priori and its value has been checked trough the relationship within the coefficient and the strain indicator value. If the strain indicator returns 272.5 με, it means that the friction coefficient is 0.2. This point has been now better clarified at the end of Section 3.3.

- Page 9 L40, After 800,000 cycles, is right?

Right. This was mentioned explicitly also in the original article.

3. Results
All SEM images should be added a label.

The caption of the figures are provided by information of the magnification, when necessary. Scales can be derived from the average crack sizes reported in the article. All the other micrographs are qualitative, in order to show the effect of the experimental test and the phenomenon involved.

- The wear rate should be considered when the crack growth rates are calculated. Please add some explanation.

Wear rate was determined simply by measuring the amount of material removed at each interval of 100,000 cycles.

- Figure 13, what are the horizontal and longitudinal coordinates?

Figure 13 represents the crack path. The horizontal and longitudinal axes represent a reference system that helps locate the crack path and to make an estimation of the crack size. For this reason the y-axis represent the distance from the surface (depth of the crack), while the x-axis represents the longitudinal “development” of the crack, starting from the first initiation point on the surface (length of crack). The Reviewer can refer to Figure12: Figure 13 is a kind of Figure12 but depicted in a coordinate system. The Figure has been now updated with these details.

- Figure 15, the image is not clear. Please revise.

Figure 15 has been replaced by a higher resolution image.

Graphical Abstract

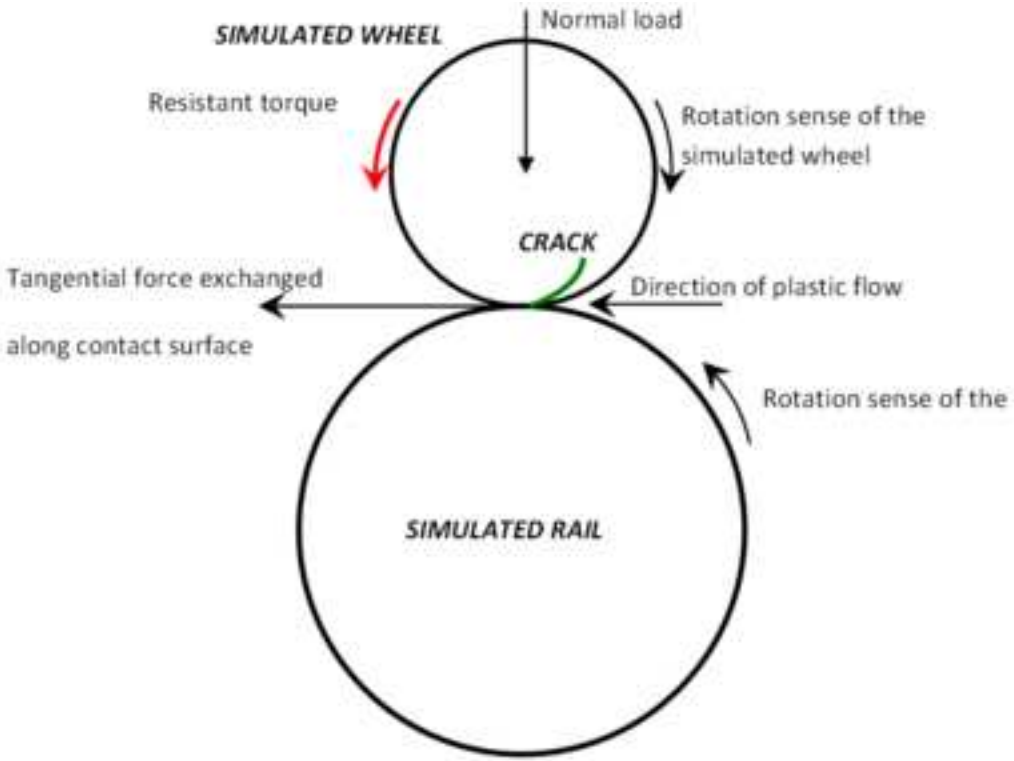

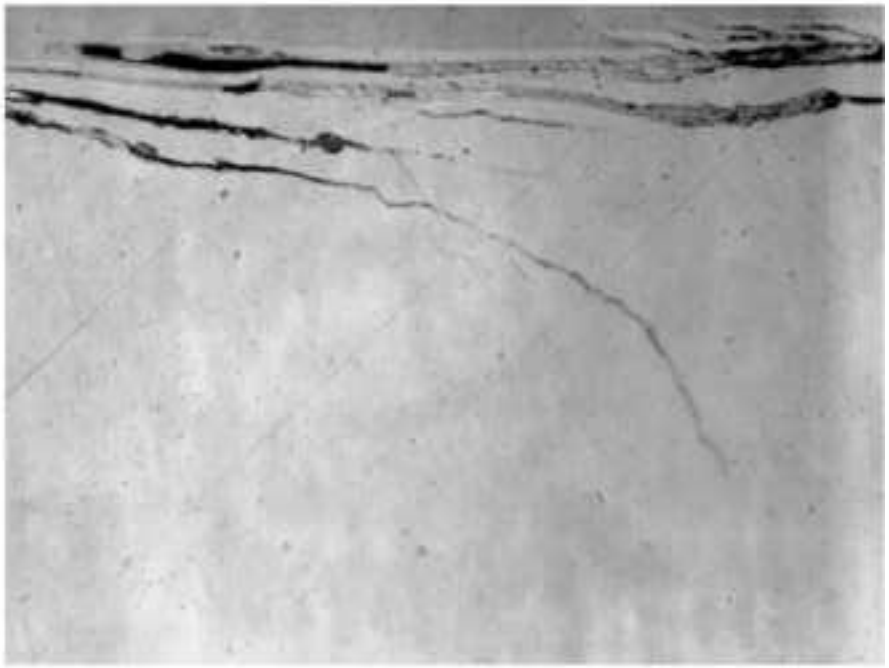

Cross section of the simulated wheel, parallel to track

***Highlights**

- Surface damage in railroad wheels is a very complex phenomenon and the contact fatigue plays a fundamental role in the damage process. Purely numerical or analytical studies will not be correct if they are based on the usual assumptions of material homogeneity and isotropy on which continuum mechanics approach relies.
- An experimental approach to evaluate rolling contact fatigue of six different materials employed in rail wheel constructions was developed in this study.
- Laboratory conditions were successfully scaled to actual railroad conditions and crack formation/propagation mechanisms were analyzed on a statistical basis.
- The materials considered in the present paper have a memory that keeps record of the previous stress/strain history and the crack propagation will be depending on such history.

EXPERIMENTAL EVALUATION OF ROLLING CONTACT FATIGUE IN RAILROAD WHEELS

C.A. Sciammarella[1], R.J.S. Chen[1], P. Gallo[2,3*], F. Berto[3,4], L. Lamberti[5]

[1] *Illinois Institute of Technology, Dept. Mechanical, Materials and Aerospace Engineering, 10 SW 32nd St, 60616 CHICAGO USA*

[2] *Aalto University, Department of Mechanical Engineering, Marine Technology, Puumiehenkuja 5A, 02150 Espoo, Finland*

[3] *University of Padova, Department of Management and Engineering, Stradella San Nicola 3, 36100 Vicenza, Italy*

[4] *NTNU, Department of Engineering Design and Materials, Richard Birkelands vei 2b, 7491 Trondheim, Norway*

[5] *Politecnico di Bari, Dipartimento di Meccanica, Matematica e Management, Viale Japigia 182, 70126 – BARI, ITALY*

sciammarella@iit.edu, pasquale.gallo@aalto.fi, filippo.berto@unipd.it, luciano.lamberti@poliba.it

Abstract

Surface damage in railroad wheels is a very complex phenomenon and the contact fatigue plays a fundamental role in the damage process. In the case of railroad wheels the actual fracture process is quite different from the conventional idea of fracture in a load bearing structural component. The cracks that are generated by contact fatigue are not the source of actual wheels cracking but lead to the damaging phenomenon called shelling which implies separation of chunks of material from the surface. Shelling is mainly due to the presence of a fluid in the contact area, which penetrates in the fatigue cracks and causes a crack propagation leading to the separation of a portion of the wheel surface. A basic starting point to analyze this phenomenon is to study the crack development in the contact surface and to evaluate the behavior of different types of steels used for wheels manufacturing. However, the challenge to obtain a reliable similitude between laboratory and real conditions is far from straightforward.

The present paper illustrates an experimental approach for rolling contact fatigue and shelling evaluation based on the possibility of simulating, in the laboratory, boundary conditions that can be scaled to the actual railroad, thus providing a realistic evaluation of the contact fatigue life of different steels.

Key words: Rolling contact fatigue; crack propagation; fatigue; rail vehicles; railway engineering;

***Corresponding author:** pasquale.gallo@aalto.fi

1. INTRODUCTION

Wheel-rail interface and, more in general, the rolling fatigue, has been a really attractive research topic for several years, simply consider that the first stretch of a railway line with locomotives and regular traffic was opened in England in 1825. In that period, massive railway projects were launched in many countries all around the world [1], such as in Sweden and Norway. The improvement of this complex and fascinating machine has never reached a break, leading today to superlative examples of cutting-edge technology, e.g. Japanese Shinkasen and French TGV that can easily reach speed higher than 300 km/h. The design of these machines is anything but easy and different aspects still result critical nowadays. One of them is the wheel-rail contacts. For the wheel-rail interface, the pioneering scientific breakthroughs occurred in the 1880s. Worth mentioning Heinrich Hertz, who proposes a theory of elastic contact that found soon application in railway engineering, followed by other researchers, and August Wöhler, in the 1850s, who studied the fatigue phenomenon in the case of railway axes. The fundamental theory of rolling contact fatigue instead was published in 1947 by Gustaf Lundberg and Arvid Palmgren. Their application was rolling bearings [2].

From those pioneering works, higher speeds and greater axle loads are creating more demanding operating conditions for the wheel-rail interface, while in parallel, development of advanced numerical models and computer based simulations, led to a refined adhesion control of traction and braking, with optimization of the wheel-rail interface followed by new and different problems [1]. In the contact zone, indeed, several undesired phenomena may occur: high vertical contact forces, but also lateral and longitudinal forces, induce stresses that may cause material yielding and fatigue; rolling contact forces combined with friction induce wear; traction and breaking may lead to wheel sliding resulting in rail burns and wheel fault, unfavorable material phase transformations, and thermal cracks [1]. Different phenomena to be faced with involve different research fields: contact mechanics, material mechanics, tribology and dynamics, railway noise, vibration, rolling contact fatigue and fracture mechanics are examples of the most “traditional fields”. Among them, rolling contact fatigue (RCF) manifests itself in crack formation and crack growth in the material close to, or at, the wheel-rail interface. Crack initiation can occur in the surface, normally due to severe plasticization, and at a subsurface level (from microstructural defect). The study of RCF, through the fracture mechanics, is far from straightforward. In fact, several complicating factors are involved, e.g. complex states of stress and strain, crack face friction and anisotropic material, fluid entrapment in the crack. It is well known that considerable studies on RCF in rail have been conducted, but some lack in our knowledge still exist, for example: crack initiation and wear, crack propagation by contact

stresses, crack propagation controlled by bending stresses. It should also be mentioned the challenge to obtain a reliable similitude between laboratory and real conditions.

The complex phenomena presented in the introduction have been considered by different authors also in the recent literature, briefly recalled below.

In the work by Kondo at al. [3], a study on the shelling phenomenon affecting Shinkansen trains was presented. In that original work, discussion of the causes and applied counter measures of shelling were presented. Despite the deep analyses and discussion of the results, the mechanics of shell formation was not well understood.

An interesting work regarding rail rolling contact fatigue was presented in Ref. [4]. The paper summarized the state of the art and a review of the research program of the "European Rail Research Institute". Laboratory experiments were conducted on small scale rotating test pieces and on full scale rolling wheel on rail tests. Despite several difficulties experienced, RCF damage was produced but laboratory testing to simulate service rolling contact conditions remains problematic.

A comprehensive review was recently presented by Sadeghi et al. [5] regarding RCF of bearings. In that paper, some of the most widely used RCF models were reviewed and discussed, and their limitations addressed. The paper also presented a new model developed by the authors considering a non-homogeneous microstructure of randomly shaped, sized and oriented grains.

An investigation of the effect of train curving on wear and contact stresses of wheel and rail was conducted in [6]. The authors focused on the stresses due to the wheel/rail contact, on the wear and on the effect of railway vehicle curving. A sophisticated numerical method was presented and it was found that the material wear volume per length along the rail running surface had a tendency to grow. The wear changes the profiles of the wheel and the rail, and leads to the serious problems, but, the wear can efficiently eliminate small cracks on the rail running surface, and suppress the growth of the cracks. Based on that principle, railway companies scientifically grind the rails in service to relax the contact stresses, eliminate and reduce the rolling contact fatigue of the rails.

RCF crack growth was analyzed in detail by Zhong et al. [7] in terms of chemical composition, mechanical performance and microstructure. The crack propagation in rails under RCF is of vital importance for the railway industry. Some authors tried in the past to develop tools for crack growth prediction. Numerical simulations of crack growth in rails were proposed in Ref. [8], focusing on short surface head check like cracks, often observed at the rail gauge corner. The result suggested that anisotropic effects from the highly deformed surface layer may need to be included in order to simulate head check growth in rails accurately.

Some attempts to model rate of wear and RCF on the wheel were also made recently [9,10]. For example in Ref. [10], the development of a damage model to predict the deterioration rates of the wheel tread considering wear and RCF was presented. The damage model was previously validated using observation data on different vehicles. Despite the good results, further analysis are required to understand the influence of parameters involved on wheel damage (e.g. traction and braking, wheel slide protection systems efficiency).

In order to study the effect of tangential force on wear and rolling contact fatigue behaviors of wheel material, experimental tests were conducted by He et al. [11] recently. Surface damage behavior observations permitted to assess the influence of tangential force on RCF and wear.

Interactions between RCF and wear of rails were recently analyzed by Seo et al. [12]. The test specimens did not have the same dimensions of the real components, but were taken from the rim of a wheel and the head of the rail. To reproduce material surface conditions of a real-sized wheel and rail using the small-sized specimens, a series of heat treatment processes were applied. Also the surface roughness of the rail was reproduced.

The competitive relationship and interaction within rolling contact fatigue damage and wear was also considered and presented by different authors, e.g. see Ref. [13-15]. An attempt to realize experimental tests that represent the real working conditions of wheel-rail contact was made by Mazzù et al. [16]. RCF tests were carried out on cylindrical discs with diameter of 60 mm and 15 mm thick. Other interesting papers have been presented by the same authors regarding numerical approaches, models, and failure assessment of rolling contact fatigue and wear [17–20].

The previous discussion demonstrates that rolling contact fatigue of railroad wheels and the related experimental simulations still represent a fundamental and attractive research topic. In view of this, the present study aims to investigate the reasons for heavy damage of truck wheels in a particular railroad service region where the tonnage is steadily increased (mean axle load 37 tons). Another objective is to properly evaluate a variety of steels and thermal treatments in order to improve fatigue life of wheels. Rolling contact fatigue was evidenced by the formation of shallow shells. However, it was not clear the mechanism of the crack formation and propagation. Preliminary analysis of early damage of wheel's surface showed parallel cracks at very regular intervals perpendicular to the rolling direction (about 1 mm apart). A typical cross-section of the cracks parallel to the rolling direction (see Figure 1) shows a crack propagating initially in mode II, and finally approaching mode I until the crack propagation is stopped by a reduction of the stress. From these observations it was concluded that the damage of the wheels was not the result

of the typical contact stresses damage caused by rolling, since cracks seem to start at the surface and not at the level where the shear stresses are maximum (as it occurs in roller bearings).

2. APPARATUS AND EXPERIMENTAL DETAILS

2.1 Experimental set-up

The experimental set up was realized in order to investigate the rail-wheel RCF problem and provide the capability of material evaluation, reproducing in the most faithful way the real conditions affecting real wheels. It must be pointed out that, because of the vast complexity of the problem under analysis, costs restraint effective research and represent an important factor to be considered in experimental determinations.

The actual distribution of contact stresses is very complex and statistical in nature. The characteristics of the wheel that have an important effect on the stress field are: shape design (this is a trade-off between steering capabilities and fatigue), wear requirements (these variables define the stresses distribution), adhesion creep characteristics of wheel material, development of residual stresses due to plastic work-hardening, presence of thermal stresses generated during braking. These characteristics are quite complex and depend on a large number of variables. Wheel and rail are envelopes of each other and their relative profiles are continuously changed by wear and by resurfacing that is part of the maintenance work. In order to simplify the problem, a wheel-rail simulation device was designed and built in this study. The testing apparatus, shown in Figure 2, includes the following components:

- Small wheel (simulated railroad wheel) riding on a larger wheel (simulated rail);
- DC motor coupled with a reducer;
- Continuous speed controller;
- Belt transmission system;
- Magnetic pick-ups and electronic counter;
- Pneumatic brake;
- Brake control unit;
- Torque measuring device;
- Steam supply unit;
- Digital counter.

The wheels are shown in Figure 3. The simulated wheel may be represented by a cylindrical surface, while the simulated rail is represented by a circular cross section. The wheel was accurately designed in order to reproduce elastic Hertzian contact normal stress distribution, derived from a 100 ton train car. The assumption of the Hertzian theory is a well-established

procedure when dealing with rail-wheel contact problems as shown in the references given in the introduction. The normal load was applied to the small wheel by a cantilevered gravity loading system through a fork holding the small wheel bearings.

The rolling speed of the wheels was monitored through the continuous speed controller.

Magnetic pick-ups (number 6 in Figure 2) served to measure the individual rotating velocities of the wheels and the electrical outputs were fed to an electronic counter that yielded the individual speeds and the speed's ratio with four significant figures. A friction force was applied by braking the simulated wheel with a pneumatic brake. The applied torque was measured by a strain-gage torque sensor. The braking torque was calibrated as a function of the applied pressure.

2.2 Important aspects of the set-up design and performance

The experimental set-up was designed on the basis of previous experience accumulated in performing tests with larger facilities. The idea was to simulate the real operating conditions as closest as possible within reasonable limits. The basic starting point is suggested by the theory of similitude, getting the same initial Hertz contact stresses with the same materials used in the actual wheels and rails. The contact between wheel and rail changes drastically as the rolling takes place [21–23]. The wear and the plastic deformations change the initial Hertz ellipse to an almost rectangular area of contact. The width of the contact area is determined by the profile radius and the wear rate. The width increases as the wheel rolls until a state of equilibrium is reached and changes in the contact area become minimal.

The effect of the different variables such as adhesion, creep, normal, tangential loads, roughness has been analyzed and found to be consistent with previous observations conducted in the past [24]. One important conclusion is that the product of the area times the creep remains a constant for a given value of the normal load P, friction coefficient μ and critical coefficient μ_c, where this is the maximum coefficient of friction that is used to derive a dimensionless creep curve. As a consequence of this observation, measurements were carried out after a fixed number of cycles required for a stabilization of the contact area. From that point it was checked that the contact area remained constant within a certain standard deviation depending on the particular material used in the simulated wheel. The rail material instead was not varied. In freight railroad track a wheel passes over a particular portion of the track within a period of time. During this time the rail surface oxidizes and the rust formed prevents a direct metal to metal contact between wheel and rail. In the laboratory tests, experimental conditions prevent formation of dust thus leading to the possibility of direct metal-to-metal contact generating phenomena such as cold pressure welding, vibration and slip. In order to avoid all these problems it was injected a

small quantity of dry vapor, avoiding undesirable phenomena like water penetration in the surface formed crack.

2.3 Testing procedure

Six different materials have been considered and two wheels for each material have been tested according to the procedure described in the previous section. They are designated as C, D, E, F, G, U. Summarizing test conditions:

- Constant normal load P = 242.4 N;
- Same tangential load T = 0.2 x 242.4 = 48.48 N;
- Same geometries of simulated wheels and rails (see Figure 3);
- Same environment;
- Same roughness (0.0003 CLA).

The following data were collected every 100,000 cycles:

1) *Contact area*.
2) *Crack density*. The crack density was determined by counting cracks in the observed regions. For each material two wheels were studied and 20 pictures were taken. The images were taken with 50X magnification. A microscope with a 10X objective and numerical aperture 0.25 was utilized. The objective has a resolution of 1 μm. An 5X ocular was used and a camera with an additional magnification of 4X was used to get micro-photographies of size 0.4775 mm x 0.365 mm. To standardize the test, 10 μm was considered the crack initiation length. With this procedure, ensemble average of crack density was calculated every 100,000 cycles.
3) *Crack length*. The formed cracks are curved surfaces which can roughly considered as elliptical. The measured crack length is therefore only the crack propagation on the surface.

Once the test stopped (every 100,000 cyles), the following operations were performed on the wheel and rail:

1) The wheels were removed; the sense of rotation of the small wheel was saved using a marking arrow.
2) The simulated wheel (SW) was cleaned with methanol and then in an ultrasonic bath.
3) The SW was weighted in an electronic balance with an accuracy of 0.0001 g.
4) The SW was mounted in a Vernier-rotating stand for observation with a microscope. The track surface was observed and 10 micrographs were taken 36^{o} apart.
5) The simulated rail was resurfaced to keep the original radius and polished to the initial finishes.

The experiments were performed as described for 700,000 cycles. In addition to the above tests for crack analysis, more 100,000 cycles were added for pitting damage investigation. In this case, the vapor was replaced by water drops to induce pitting due to the water pressure. The water test was conducted on wheels that have already been cracked. In the actual wheels and rails the presence of liquids influences the already cracked wheels; the liquid is an additional factor that adds a load to the existing crack.

After 800,000 cycles, the small wheel was subjected to metallographic analysis using cross-sections parallel to the rolling direction. A 3% Nital (alcohol and nitric acid) solution was used to etch the specimens. Regarding the pitting tests, SEM images of the specimens were taken.

2.4 Material properties

Six high strength steels for rail constructions were tested in the experiments, and are here classified as a function of their hardness. In detail: the initial C-Rockwell hardness, the Knoop micro-hardness outside the track area after the tests (HK-Out) and the Knoop micro-hardness inside the track area after test (HK-In) are given in Table 1. Materials C, D, E and G are harder than materials F and U. Materials and specimens were provided by manufacturers as the representative elements that they use in the manufacture of the corresponding parts.

As far as it concerns changes experienced by the material during testing the following measurements were taken:

1) The rims of the simulated wheel and the simulated track were subjected to C-Rockwell measurements.
2) All the wheels were subjected to micro-hardness tests, both in the contact region and outside the contact region.

3. TECHNIQUES FOR DATA ACQUISITION PROCESS

The accuracy and reliability of the presented results depend in large extent on the techniques involved in the data acquisition process. Some of the techniques involved in this paper were developed and improved at the Illinois Institute of Technology (Chicago, USA) and are presented in the following subsections in detail.

3.1 Measurement of the contact area between rail and wheels

This task was accomplished by using a 4 mil (i.e. 102 μm) replicating transparent tape placed between simulated rail and wheel. The replica technique is based on a similitude law between the replica left on the tape and the actual contact area as predicted by the Hertz theory. This

technique has been verified in the measurement of the contact areas in reduced scale models as well as in actual railroad wheels.

3.2 Measurement of the rolling speeds and relative sliding.

The speed of rotation was measured with magnetic pick-ups with a resolution of 1/144 of a revolution. The following equation has been adopted:

$$\xi = 1 - \frac{R_S N_S}{R_B N_B} \tag{1}$$

where ξ is the longitudinal creep; R and N, respectively, indicate the radius and the number of revolutions of the wheels per unit time; the subscripts S and B indicate the small wheel (simulated wheel) and big wheel (simulated rail), respectively. Study of the accuracy of the measurement of the creep can be found in [24].

3.3 Measurement of the coefficient of friction.

The coefficient of friction was determined from the following relationship:

$$\mu = \frac{T}{P} \tag{2}$$

where P is the normal force and T is the tangential force. A torque meter based on strain-gages senses the torque applied by the brake. This torque is directly proportional to the coefficient of friction between the two wheels as long as slip between the two wheels does not occur. This condition can be verified easily by observing the velocity counter. A calibration was performed by applying a known torque. The following equilibrium equation can be written,

$$T \cdot R_S = Q \cdot L_B \tag{3}$$

In this equation, T is the tangential force applied to the small wheel surface, R_S is the radius of the small wheel, Q the force that multiplied by the lever arm L_B gives the value of applied torque. Since $T = \mu P$, where μ is the coefficient of friction and P is the applied normal force, it follows from Eq. (3),

$$\mu = \frac{L_B \cdot Q}{R_S \cdot N} \tag{4}$$

Calibration was performed and thus μ becomes a function of the reading of the strain-gage bridge. Being available the relationship within the friction coefficient and the strain-gage bridge, an indirect measurement of the coefficient has been made possible during the test.

In detail, first a desired value of the friction coefficient has been imposed a priori, that is μ=0.2. In turn, the corresponding value of the strain indicator, that is 272.5 με, has been determined. Knowing the target of strain indicator value that assures the desired friction coefficient, during the experimental testing the value reported by the strain indicator has been checked to be as much close as possible to 272.5με, implying a controlled value of the friction coefficient close to 0.2. The variation of the measure has been also quantified in a 0.7% variation of the friction coefficient.

4. RESULTS

Because of the complexity of the CRF phenomena, different parameters were observed and related issues are briefly reported below for the sake of clarity. Extensive comments for these results are reported in a specific section later in the manuscript.

4.1 Contact area, ensemble average-crack density and surface average crack length

Figure 4 shows the measured contact area as a function of the number of cycles. Material U exhibited considerable dispersion while contact area remained close to the initial value for the other materials.

The ensemble average crack density of the different materials is plotted in Figure 5; trends show very little dispersion. Figure 6 shows the surface crack length density for the different materials. This quantity shows a regular progression with the number of cycles. Both data series were fitted by a 3-parameter Weibull distribution following Eq. (5):

$$F(N) = A\left(1 - e^{-CN^{\beta}}\right) \tag{5}$$

where N is the number of load cycles. The parameters A, C and β were determined by best-fitting experimental results: for that purpose, the Newton-Raphson method and a least square method were used. It appears that experimental data are very well fitted by the Weibull distribution: in fact, the average error made in the fitting operation ranges between 0.970% (material D) and 3.218% (material G) for the number of cracks, and between 2.274% (material C) and 5.024% (material F) for the crack length, respectively.

The crack density value is taken as an ensemble density distribution of events, the random formation of an individual crack due to the presence in the material of sources of damage initiation (weak links). At the end of the process there is a saturation in the number of cracks when the different cracks begin to interfere with each other and the process of crack creation and propagation slows down to a holt. A similar thing occurs with the density of crack length per unit area of the surface. The stabilization of the process means that the weak points at the surface neighborhood have been exhausted because of the prevailing stress level, and cracks have grown to dimensions such that they begin to shield one another. It is necessary an external factor, such as the presence of fluids on the track, to propagate a crack.

4.2 Wear

Wear is the loss or displacement of material from a contacting surface. Figure 7 shows the variation of the wear of wheels with respect to the number of cycles. It can be seen that wear increases linearly as load cycles progress: the correlation coefficient R^2 computed for linear fitting ranged between 0.934 (material F) and 0.997 (material G).

Considering the effect of wear on the crack initiation, there are two different active mechanisms of damage: surface damage due to the presence of very high stresses caused by local contact interferences of surface irregularities, and surface damage caused by global stress. The first produces the removal of superficial layers, while the latter generates deep penetrating cracks. The accurate observation of the tested surfaces showed the presence of both mechanisms.

The number of cracks as a function of the wear is depicted in Figure 8. This curve shows the effect of the hardness on the number of cracks generated. There are two mechanisms operating: crack generation and crack removal. The former predominates in harder materials. This is proven by Figure 8 which shows that for a given amount of wear the number of cracks is larger in the case of harder materials. Since wear linearly increases with the number of load cycles, Weibull distribution can precisely fit these data: the average error made in the fitting operation ranged between 0.989% (material D) and 3.23% (material G).

Figure 9 illustrates the effect of wear on crack length density L_A. This effect becomes less significant for softer materials while harder materials show larger values of crack length density. Weibull distribution fitted very well also these data: average error ranged between 2.30% (material C) and 5.38% (material F). This is another consequence of the linear relationship between wear and number of load cycles.

Figure 10 shows the variation of $\partial N_{CR}/\partial W$ (number of cracks/mg) with respect to the number of cycles: it can be seen that (i) such a rate decreases as fatigue loading progresses and (ii) softer materials present lower rates than harder materials. Weibull distributions fitting

experimental data also are plotted in the figure in order to have a homogeneous basis of comparison with the previous figures. It can be seen that the Weibull model fits experimental data far less accurately than in the case of number/average length of cracks vs. number of cycles/wear data (see Figures 5-6 and 8-9). In particular, the Weibull model was found: (i) to cover the entire range of load cycles considered in the experiments only for materials E and U (average errors between 8% and 11%), (ii) to be reliable only in the first half of fatigue life (i.e. until 300,000/500,000 cycles) for materials C, D and G (errors between 9% and 14%), (iii) not to be valid for material F. The data plotted in the figure were instead best fitted by inverse logarithmic (materials C, G and U), negative exponential (material D) and power functions (materials E and F); the corresponding correlation coefficients R^2 ranged between 0.887 and 0.979. The non-Weibull best fits for materials E and U are included in the plot: the former yields $R^2 = 0.951$ and crosses the corresponding Weibull fit at 400,000 cycles while the latter yields $R^2 = 0.887$ and is very close to the corresponding Weibull fit.

Figure 11 shows the variation of $\partial L_A/\partial W$ (mm/mm^{2}mg) with respect to the number of cycles. It can be seen that length change rate again decreases significantly with the number of revolutions. Weibull-based fitting is yet less accurate than before, mainly because $\partial L_A/\partial W$ is a rather small quantity which hence is more sensitive to numerical noise. This is confirmed by the fact that the whole range of load cycles considered in the experiments could be covered only for material E with an average error of 13%; errors for materials C, D and G ranged between 12% and 22% for the first 300,000/400,000 cycles performed in the tests; Weibull distribution could not fit experimental data for materials F and U. The data plotted in the figure were instead best fitted by negative exponential (materials C and D), power (materials E and F) and inverse logarithmic (materials G and U) functions; the corresponding correlation coefficients R^2 ranged between 0.908 and 0.982. The non-Weibull best fit for material E is included in the plot: it yields $R^2 = 0.908$ and practically coincides with the corresponding Weibull fit.

5. DISCUSSION OF THE RESULTS

5.1 Significance of experimental tests

The purpose of this work was to simulate as close as possible the operating conditions that occur in an actual railroad wheel. The initial damage of an actual wheel is shown in Figure 1 and is a typical crack observed in the wheel tread. Figure 12 shows a crack formed in the simulated wheel after $8 \cdot 10^5$ rolling cycles. Figure 13 shows a representation in μm of the two crack profiles together with a displaced version of the crack of the simulated wheel to adjust for the distance of the crack to the tread surface. The paths of the two cracks are very similar. It can be concluded

that the adopted similitude design approach reproducing the contact area in reduced scale, that is a scale reproduction of the actual wheel contact ellipse and yields the same stress level, has worked out well. Consequently, the wheel model gives a realistic picture of the processes occurred in the field. However, some differences should be pointed out.

The surface crack growth in the small wheel is limited to approximately the width of the track. In the initial conditions, the minor axis of the contact ellipse is 460.1 μm. The maximum crack length observed in a microscopic view was on average 270 μm, that is of the order of magnitude of the crack width. The total length of the crack represented in Figure 13 is 217.5 μm. Consequently, one can assume that the deepest crack observed experimentally is a curved surface in space with develops on the surface and in depth almost by the same extent. In the actual wheel, the minor axis of the contact ellipse is 5.659 mm and the surface crack length observed covers the entire region where the contact between the wheel and the rail takes place. It should be remembered that the contact regions in actual wheels move thus covering a wider area than the contact area. Also the tangential load is not applied all the time, but takes place during braking and curving. The profile of Figure 1 is typical of the crack depth observed in the actual railroad wheel; it has practically in depth the same geometry and the same length than the simulated wheel but corresponds to three orders of magnitude larger number of cycles. Roughly it can be said that the life of the model wheel of $8 \cdot 10^5$ corresponds to $1.1 \cdot 10^8$ cycles of the actual wheel. Furthermore, the crack length observed in the actual wheels on the surface is much longer than the contact area. The crack ceases to propagate in depth after a certain number of cycles but can still propagate on the surface.

Of course, this is one single set of observations but it gives an idea of the correspondence between an actual wheel and a simulated wheel in the laboratory. The laboratory test can be considered as an accelerated test but still provides good clues on the mechanism of crack formation and the response of different materials and thermal treatments to the service conditions.

5.2 Damage mechanism

In order to understand the process of wheel damage, first it is necessary to analyze the actual observed phenomena. Figure 14 shows a schematic view of the testing set up. A tangential force is applied to the model wheel in the direction of rotation and this force causes plastic flow in the direction of the applied force.

Figures 15 and 16 show cross sections taken parallel to the track. From these micrographs of the metal follows that very large plastic deformations take place up to about 200 μm in depth.

The magnitude of the deformations can be estimated from the changes in dimensions of the steel grains and of the texture of the surface. In a railroad wheel the contact stress distribution is very complex and depends heavily on the friction forces between the two contacting surfaces and on the applied tangential forces. There is an adhesion region and a slipping region: the former corresponds to the front part of the contact area. The size and position of the adhesion zone depend on the normal and tangential forces applied to the wheel. It is in this adhesion zone where the larger plastic deformations take place.

Generally speaking, the basic issue in understanding the actual physics of the contact is to identify the adhesion region and the slipping region. These two regions always exist if the contact has friction. In the adhesion region the two materials deform together by molecular adhesion. In the slipping region the two materials have relative displacements that in the railway nomenclature are called creep. If we have a symmetric surface, separation between the two areas will have the same symmetry. For example, if the contact area is a circle (such as in the case of the contact involving a spherical surface), the separation will be a circle. Similarly, if the contact area is an ellipse (such as in the case of the contact involving a cylindrical surface), the limit between the adhesion and slipping regions will be an ellipse.

A previous study carried out by the first author considered the case of a semi-spherical ball of highly polished steel in contact with a simulated infinite plane made of plexiglass [25,26]. The moiré technique [25] was used for analyzing contact stresses developed under static normal load and friction. The experimental set up utilized in those experiments is shown in Figure 17-a. The plane containing the grating is the plane of symmetry of the plexiglass prism. The contact region in this case is a circle; because of symmetry, the 3-D distribution of stresses can be studied in 2-D, in the symmetry plane where the XY reference system is set. As expected, friction changed distributions of normal/shear strains with respect to the classical Hertz's solution. Figures 17b-d illustrate the presence of the two regions: the region of low shear corresponds to the adhesion area while the pic area corresponds to the slipping region.

As the contact becomes dynamic the symmetry of adhesion region and slipping region disappears. This is confirmed also by a previous study carried out by the first author [27] where residual strains caused by rail-wheel contact were measured with the moiré method. A model wheel (the same as that used in the present study but with a flat surface rail of curvature radius equal to infinity) was applied to a rail where a cross grating was engraved. The wheel was subjected to a normal force and a tangential force. The grating was deformed because of the rail-wheel contact and analyzed using the moiré method. The lines of principal plastic strains corresponding to contact with normal force and a torque were obtained from the study of the

moiré pattern and correspond to the residual plastic deformations left by the effect of the rolling contact in the rail. It can be seen that the front part of the wheels experiences very high strains as indicated by the residual strains left by the applied forces (see Figure 18-a). These strains are in the direction of the rolling. In the transversal direction also there are very large permanent strains (see Figure 18-b). Although it is an idealization of the process of contact it provides useful information concerning the size of the adhesion region and the slipping zone.

Figure 19 gives another clue on the development of the rolling contact process. It comes from experimental measurements made by impending rolling [28,29], corresponding to a cylindrical wheel [30]. Moiré techniques were used for measuring displacements and strains caused by contact. In the figure, actual measured strains have been scaled to make the visual comparison clearer. The values given in [28,29] correspond to the center line of the contact area while the values measured in [30] correspond the centerline of the contact ellipse. Since dimensions of the major axis of contact ellipse depend on the load and materials, the position of points is normalized by making the half axis equal 1.

Figure 19 is the equivalent of plotting the strain ε_{xx} of Fig. 17: it shows that in rolling contact, the attack zone hosts high tensile stresses that are the source of the bulk cracks. It can be seen that there is a qualitative agreement between the strain distributions of the cylindrical roller [28,29] and the residual strains measured for the cylindrical wheel [30], in spite of the difference in materials (the cylindrical roller was made of plexiglass and the supporting plane was made of urethane rubber). In the contact region there is an adhesion zone, which in Figure 17-b corresponds to the region limited by the points where strain ε_{xx} becomes equal to zero (and then becomes positive) and the slip region, which is the rest of the contact area. Due to the symmetry of the problem in this case the adhesion and the slip regions are concentric.

The effect of the tangential force is to displace the adhesion zone where longitudinal strain became positive to the front of contact area (“attack region”) as it is shown in Figure 19 (according to the sketch of Figure 18, the attack region corresponds is the right edge of Figure 19). As the wheel rolls subjected to tangential force, an element of volume enters the contact area and experiences large contact forces that produce high tensile stresses and low to moderate normal forces. Then, it experiences increasing compressive stresses that go down as the element leaves the contact area. From the micrographs one can see that the cracks penetrate a region that is not isotropic but has a layered structure and is heavily damaged and slowly changes with the depth.

Another clue of the process of crack formation and growth can be obtained from Figure 20 [31]. This photoelastic pattern was obtained for a two dimensional plate representing an infinite

elastic half-plane loaded by a distributed force in a region of the boundary. The isochromatics are lines of equal shear stress. In Figure 20, we have added the crack profile plotted in Figure 13 matching the scale of the figure. It can be seen that the cracks approximately follow lines of maximum shear stress produced by the vertical load. However, there is also a horizontal load that modifies the contact zone as well as stress and strain distributions.

It should be noted that Figure 20 is quite relevant because there are several damage mechanisms activated by the rolling contact of two surfaces. There is a surface damage caused by the presence of roughness that through high cycle fatigue leads to the scaling separation of material (see Figure 22). A separate mechanism of damage is related to fatigue, caused by the bulk stress field leading to the formation of the cracks shown in Figures 1 and 12. This process is a classical fatigue crack propagation under a 3-D stress state. A recent experimental verification in this regard is presented in [32]. The fracture takes place along the isostatics of the stress field that are lines of maximum damage. In the present case, the lines of maximum damage are the lines of maximum shear. This explains the similitude of shape between the observed shear strains in the photoelastic pattern and the crack trajectory observed in the present experiments. The shear stresses correspond to contact stresses with friction and are shown as additional information to help the reader to visualize the stress field that prevails in the contact problem.

If one wants to describe crack mechanics, the anisotropy and the damage process cannot be neglected. It has been remarked that crack approximately follows the regions of constant shear stress. The cracks on the surface are statistically perpendicular to the track and, as said before, do not grow on the surface much larger than in depth: therefore, both surface and depth crack lengths are about the same. The average speed of propagation can be easily computed: surface crack grows about 200 μm in $7 \cdot 10^7$ cycles, this gives a velocity of crack growth per cycle da/dN=0.29 nm/cycle, or roughly 3 atomic radiuses per cycle. Consequently, the crack growth rate is of the order of $3 \cdot 10^{-10}$ m/cycle. There are micro-structurally short cracks of the order at maximum of 200 μm: hence, cracks are of the dimensions of the grain sizes. Most theories on crack growth are based on the continuum mechanics approach, for example the Paris' law

$$\frac{da}{dN} = C \, \Delta k_{eff}{}^{m} \tag{6}$$

However, the material does not behave any longer as an isotropic and homogeneous material at the scales corresponding to the 200 μm cracks. The crack growth is determined by the micro-structural features of the material. The speed of propagation can be quite irregular; the crack can grow very quickly in highly damaged areas and be arrested by crystal barriers in other

regions. It should be mentioned that in the present case there were no individual cracks but there are ensemble averages of thousands of cracks. In this sense, one can apply Paris' law in its generalized form shown in Eq. (6). According to the calculated average speed of propagation, we are, in the case of steels, very near the ΔK_{th} (threshold ΔK) which is a function of the ratio of minimum to maximum stresses applied (generally referred to in the literature as R) and on the presence of structural features that tend to block the crack propagation and are characterized by some length parameter (characteristic of the material structure), and also depends on environmental variables.

There are in the literature many expressions that were derived to represent the threshold behavior and that can be fitted to a particular set of data. One can take the nominal Δk value

$$\Delta k = Y \Delta\sigma \sqrt{\pi a} \tag{7}$$

where Y is the geometric factor, $\Delta\sigma$ is the stress increment applied, a is the crack length. Although the crack has a three-dimensional nature and on the surface the square root singularity is not valid, experimental investigations (based on holographic interferometry), supporting the development of series solutions to the stresses and displacements around the crack tip then utilized to find the stress-intensity factor along the flaw border [33], show that stress intensity factor values are reasonably well described by Eq. (7).

There is a very important aspect to be considered which confirms that one should be very cautious at using the idea of plasticity when a dynamic phenomenon like fatigue is involved. Plasticity itself is a dynamic phenomenon that implies the motion of dislocations. This process implies the propagation of dislocations in waves, motion that is triggered by the loading process [34]. The material in the initial condition is elastic and as it is being loaded by the contact forces follows a stress-strain relation corresponding to a 3-D stress condition. Consequently, for a given level of load, dislocations are no longer stable and begin to propagate in a plastic wave that increases the damage of the material by coalescence of the dislocations within the volume. However, since at a certain instant of time the load is reduced because of the fatigue cycle the material returns to the elastic state. This cycle repeats itself until in the damage zone coalescence of dislocations creates an actual crack that ultimately will lead to the fracture if the void created is big enough to generate the instability of the whole structure. Although the process is very complex to model, it is possible on the basis of existing knowledge to make inferences in a statistical sense as it was done in the present study.

The experiments carried out in this study show that crack generation and propagation (in particular, ensemble average-crack density and average length of surface cracks and the

quantities derived from these parameters) follow a Weibull's type statistical distribution. Variations of the rate of change of number of cracks $\partial N_{CR}/\partial N$ and rate of change of average crack length $\partial L_A/\partial N$ with respect to the number of load cycles are plotted in Figure 21. Similar to the $\partial N_{CR}/\partial W$ and $\partial L_A/\partial W$ trends shown in Figures 10 and 11 (it be must recalled that wear increases linearly with cycles), negative exponential, inverse logarithmic and power function fittings are more accurate than the Weibull distribution: in fact, correlation coefficients R^2 ranged between 0.937 and 0.975 ($\partial N_{CR}/\partial N$) or between 0.945 and 0.982 while Weibull fittings of $\partial N_{CR}/\partial N$ and $\partial L_A/\partial N$, respectively, resulted in average errors always greater than about 14% and 12% (for material E; furthermore, Weibull fit of $\partial L_A/\partial N$ practically coincides with the power function best fit). Interestingly, data relative to material E were always fitted by a power function with negative exponent values ranging between -0.823 and -0.775.

The local damage creates favorably oriented grains where the crack propagation can take place at higher speeds than those corresponding to the nominal stresses applied. As the crack penetrates in the interior of material the surface structure is less damaged. At the same time, through-depth stresses are reduced and hence the crack speed will slow down until the crack comes to rest. Considering the speed of crack length generation depicted in Figure 21-b, it is possible to see that speed goes down as the number of cycles increases.

As far as it concerns the crack length density observed in the experiments, two processes of crack generation must be highlighted. There are local contact stresses, generated by the irregular contact between the two surfaces, and global stresses. The local contact stresses cause the wear while the global stresses generate the cracks that penetrate in depth. The wear leads to the formation of debris under the form of metal flakes. This type of debris is the same in the experimental model and in an actual railroad wheel as shown in Figure 22.

The plots of the derivatives of the number of cracks and length with respect to the number of cycles, given in Figure 21, show that both the number of cracks generated per unit area and their lengths come to a steady state or a sort of a stable process. Interaction between cracks will cause shielding of the cracks. The surface cracks generated will balance with the crack removed by the wear. The longer cracks that correspond to the fracture penetrating in the wheel's ream will also slow down to a halt defining a sort of maximum density of crack formation. The situation will change if a liquid is present in the wheel that penetrates in certain cracks and finds some inner defects that will propagate cracks further inside the wheel. This situation may be helped by unusual overloads and steep braking.

6. CONCLUDING REMARKS

An experimental approach to evaluate rolling contact fatigue of six different materials employed in rail wheel constructions was developed in this study. Laboratory conditions were successfully scaled to actual railroad conditions and crack formation/propagation mechanisms were analyzed on a statistical basis. The fatigue contact problem is very complex because of the large amount of variables that need to be considered to perform the corresponding analysis. Purely numerical or analytical studies will not be correct if they are based on the usual assumptions of material homogeneity and isotropy on which continuum mechanics approach relies. However, actual observed phenomena on the basis of a statistical analysis can provide clues on the critical variables governing the damage evolution of surface fatigue.

A very important conclusion that can be drawn from this work is that for multi-axial fatigue cases like the one considered in this study the idea of damage is fundamental. The introduction of empirical quantities based on the classical continuum mechanics arguments cannot lead to adequate representation of the studied problem. One has to experimentally observe the actual events, relate them to basic mechanics formulations and then create models that must take into consideration the structural changes taking place in the material which in turn are dependent on geometrical and loading variables as well as on material properties. A material has a memory that keeps record of the previous stress/strain history and the crack propagation will be depending on such history. For example, in the particular case analyzed in the study we can see that crack trajectories can be modeled by lines of maximum shear. However, it could be not correct to state that the crack in the wheel is a mode II crack type. In fact, the possibility that all modes of crack propagation will be activated has to be addressed, since the crack trajectories will be affected by the previous stress/strain histories.

REFERENCES

[1] Lundén R, Paulsson B. Wheel–Rail Interface Handbook. Elsevier; 2009. doi:10.1533/9781845696788.1.3.

[2] Lundberg G, Palmgren A. Dynamic Capacity of Rolling Bearings. Generalstabens litografiska anstalts förlag; 1947.

[3] Kondo Yoroizaka, K., Sato, Y. K. Cause, increase, diagnosis, countermeasures and elimination of Shinkansen shelling. Wear 1996;191:199–203. doi:10.1016/0043-1648(95)06727-2.

[4] Cannon DF, Pradier H. Rail rolling contact fatigue Research by the European Rail Research Institute. Wear 1996;191:1–13. doi:10.1016/0043-1648(95)06650-0.

[5] Sadeghi F, Jalalahmadi B, Slack TS, Raje N, Arakere NK. A Review of Rolling Contact Fatigue. J Tribol 2009;131:041403 1–15. doi:10.1115/1.3209132.

[6] Jin X, Xiao X, Wen Z, Guo J, Zhu M. An investigation into the effect of train curving on wear and contact stresses of wheel and rail. Tribol Int 2009;42:475–90. doi:10.1016/j.triboint.2008.08.004.

[7] Zhong W, Hu JJ, Li ZB, Liu QY, Zhou ZR. A study of rolling contact fatigue crack growth in U75V and U71Mn rails. Wear 2011;271:388–92. doi:10.1016/j.wear.2010.10.071.

[8] Brouzoulis Ekh, M. J. Crack propagation in rails under rolling contact fatigue loading conditions based on material forces. Int J Fatigue 2012;45:98–105. doi:10.1016/j.ijfatigue.2012.06.002.

[9] Wang G, Qu S, Lai F, Li X, Fu Z, Yue W. Rolling contact fatigue and wear properties of 0.1C–3Cr–2W–V nitrided steel. Int J Fatigue 2015;77:105–14. doi:10.1016/j.ijfatigue.2015.02.019.

[10] Bevan A, Molyneux-Berry P, Eickhoff B, Burstow M. Development and validation of a wheel wear and rolling contact fatigue damage model. Wear 2013;307:100–11. doi:10.1016/j.wear.2013.08.004.

[11] He CG, Huang YB, Ma L, Guo J, Wang WJ, Liu QY, et al. Experimental investigation on the effect of tangential force on wear and rolling contact fatigue behaviors of wheel material. Tribol Int 2015;92:307–16. doi:10.1016/j.triboint.2015.07.012.

[12] Seo J-W, Jun H-K, Kwon S-J, Lee D-H. Rolling contact fatigue and wear of two different rail steels under rolling–sliding contact. Int J Fatigue 2016;83:184–94. doi:10.1016/j.ijfatigue.2015.10.012.

[13] Donzella G, Faccoli M, Ghidini A, Mazzù A, Roberti R. The competitive role of wear and RCF in a rail steel. Eng. Fract. Mech. 2005;72:287–308. doi:10.1016/j.engfracmech.2004.04.011.

[14] Wang WJ, Guo J, Liu QY, Zhu MH, Zhou ZR. Study on relationship between oblique fatigue crack and rail wear in curve track and prevention. Wear 2009;267:540–44. doi:10.1016/j.wear.2008.12.100.

[15] Ramalho A. Wear modelling in rail–wheel contact. Wear 2015;330-331:524–32. doi:10.1016/j.wear.2015.01.067.

[16] Mazzù A, Solazzi L, Lancini M, Petrogalli C, Ghidini A, Faccoli M. An experimental procedure for surface damage assessment in railway wheel and rail steels. Wear 2015;342-343:22–32. doi:10.1016/j.wear.2015.08.006.

[17] Mazzù A, Petrogalli C, Faccoli M. An integrated model for competitive damage mechanisms assessment in railway wheel steels. Wear 2015;322-323:181–91. doi:10.1016/j.wear.2014.11.013.

[18] Mazzù A. A numerical approach to subsurface crack propagation assessment in rolling contact. Fatigue Fract Eng Mater Struct 2013;36:548–64. doi:10.1111/ffe.12024.

[19] Donzella G, Mazzù A, Petrogalli C. Failure assessment of subsurface rolling contact fatigue in surface hardened components. Eng Fract Mech 2013;103:26–38. doi:10.1016/j.engfracmech.2012.05.009.

[20] Donzella G, Mazzù A. Extension to finite life of a failure assessment diagram for contact fatigue loading. Int J Fatigue 2012;44:217–24. doi:10.1016/j.ijfatigue.2012.04.014.

[21] Kalker JJ. Wheel-rail rolling contact theory. Wear 1991;144:243–61. doi:10.1016/0043-1648(91)90018-P.

[22] Wang P. Design of High-Speed Railway Turnouts. 1st ed. Academic Press; 2015.

[23] Makino T, Neishi Y, Shiozawa D, Fukuda Y, Kajiwara K, Nakai Y. Evaluation of rolling contact fatigue crack path in high strength steel with artificial defects. Int J Fatigue 2014;68:168–77. doi:10.1016/j.ijfatigue.2014.05.006.

[24] Sciammarella CA, Kumar S, Nailescu L, Seth BB. Similitude Law for the Creep-Adhesion Function in Dry Contact. J Eng Ind 1979;101:278. doi:10.1115/1.3439508.

[25] Sciammarella CA, Sciammarella FM. Experimental Mechanics of Solids, Wiley, Chichester (UK), 2012.

[26] Sciammarella CA, Bath G. Computer assisted moiré method, In: Proc. Euromechanics Colloquium No.256 on Non-destructive 3-D stress analysis, Tallin (Estonia), 1989.

[27] Sciammarella CA. *Friction Creep and Wear Studies Between Steel Wheels and Rails*. U.S. Department of Transportation, Federal Administration Office of Development and Reseach, Report N FRA-OR and D-76-271, July 1976.

[28] Bremond CH. Resolution de problems de contact elastique plan avec frottement a partir de donnees experimentales. Ph.D. Thesis, Claude Bernard University, Lyon, France, 1976.

[29] Bremond CH, Durelli JA. Experimental analysis of displacements and shears at surfaces of contact. Exp. Mech. 1981; 21:105-110.

[30] Sciammarella CA, Albertazzi A. Measurement of residual stresses by the moire method. SEM Conf. Exp. Mech., Albuquerque (NM) USA: 1990, p. 419–26.

[31] Frocht MM. Photoelasticity: Volume 2. New York, USA: John Wiley and Sons; 1948.

[32] Sciammarella CA, Casavola C, Lamberti L, Pappalettere C. Investigation on fracture behaviour of turbine blades under self-exciting modes. Strain 2011; 47-S1: e113-e129.

[33] Dally JW, Sciammarella CA, Shareef I. Extraction of Stress-Intensity Factor from In-Plane Displacements Measured by Holographic Interferometry. Surface-Crack Growth Model Exp Struct 1990;1060:130–41.

[34] Sciammarella CA, Lamberti L, Merging experimental evidence and Molecular Dynamics theory to develop efficient models of solids fracture. Proceedings of the 2016 SEM Conference on Experimental and Applied Mechanics, Orlando (FL), USA, 2016.

TABLES

Table 1. Initial HRC is the initial Rockewell C hardness; HK-Out is the Knoop micro hardness outside the track area after the tests; HK-In is the Knoop micro hardness inside the track area after the tests.

	Material					
	C	D	E	F	G	U
Initial HRC	32	33	33	19	34	17
HK - Out	255	261	247	185	261	179
HK - In	470	383	410	321	370	309

FIGURES

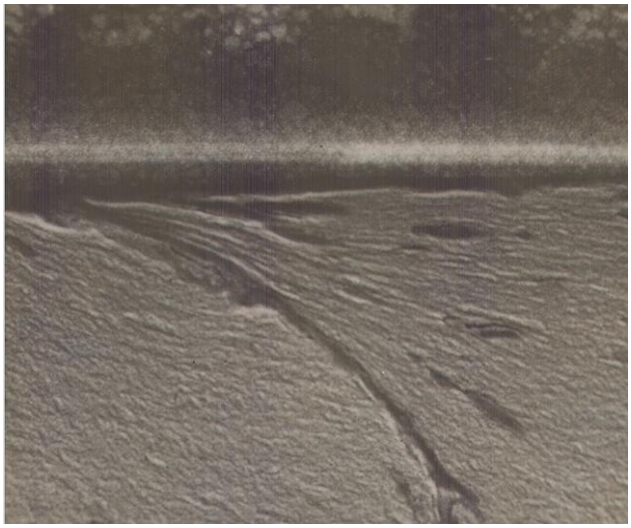

Figure 1. Fracture pattern on the actual railroad wheel

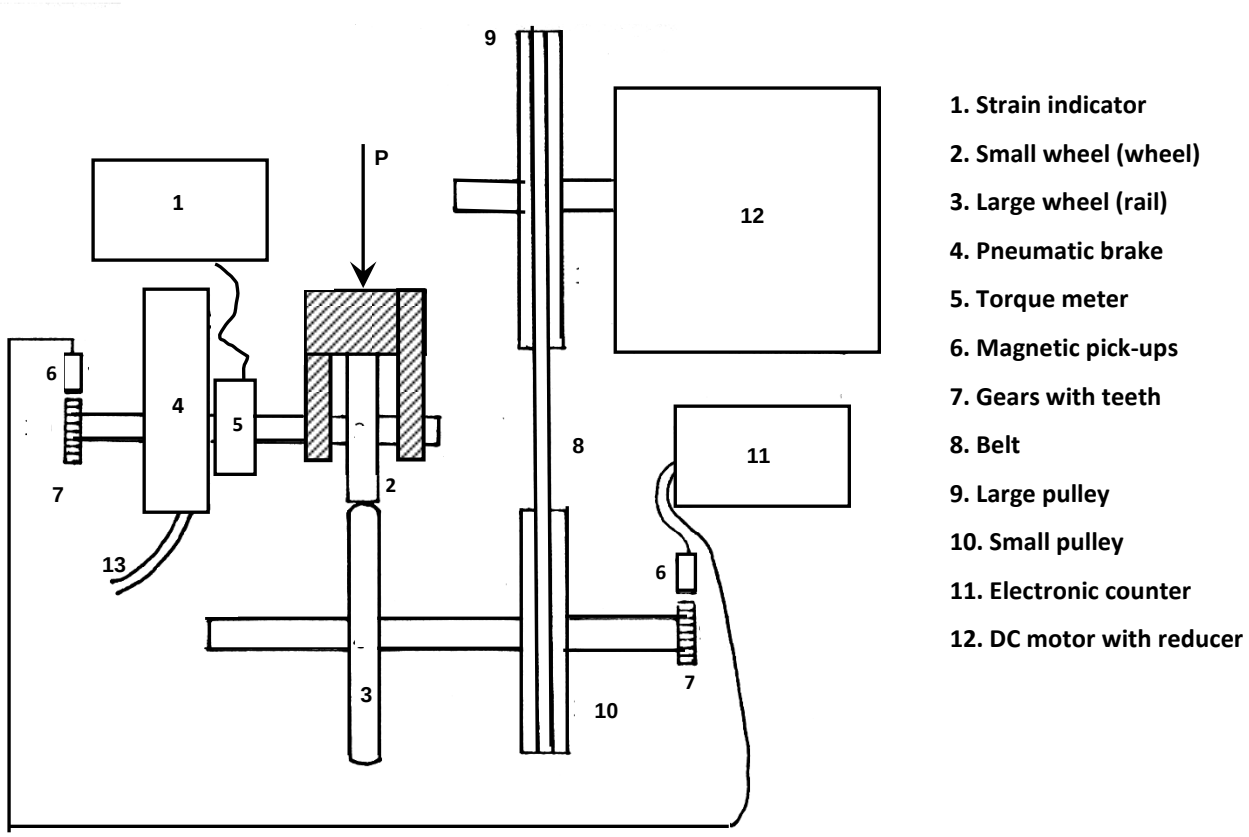

Figure 2. Schematic of the testing apparatus used to simulate the rail-wheel rolling contact

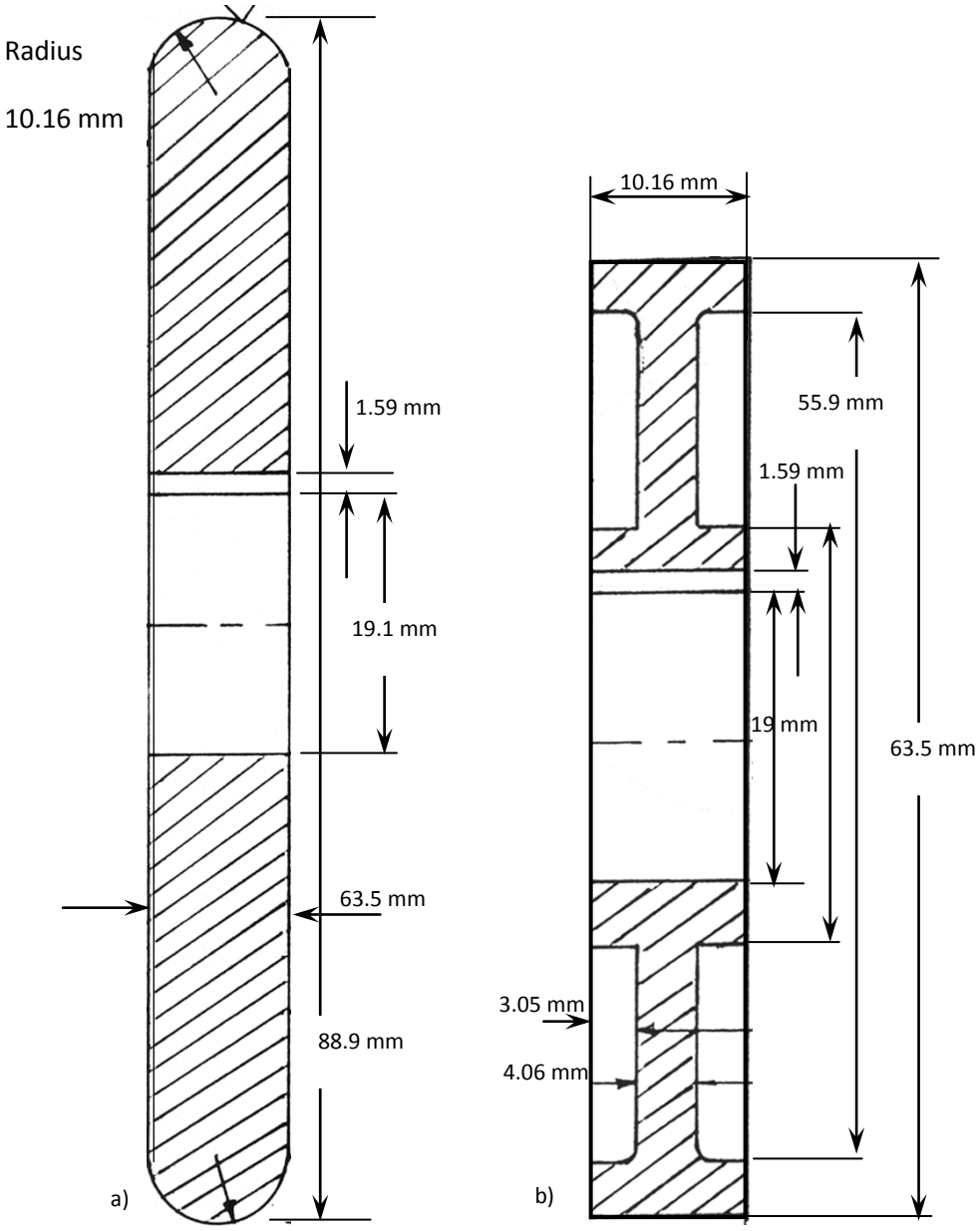

Figure 3. Schematic of simulated rail (a) and simulated railroad wheel (b)

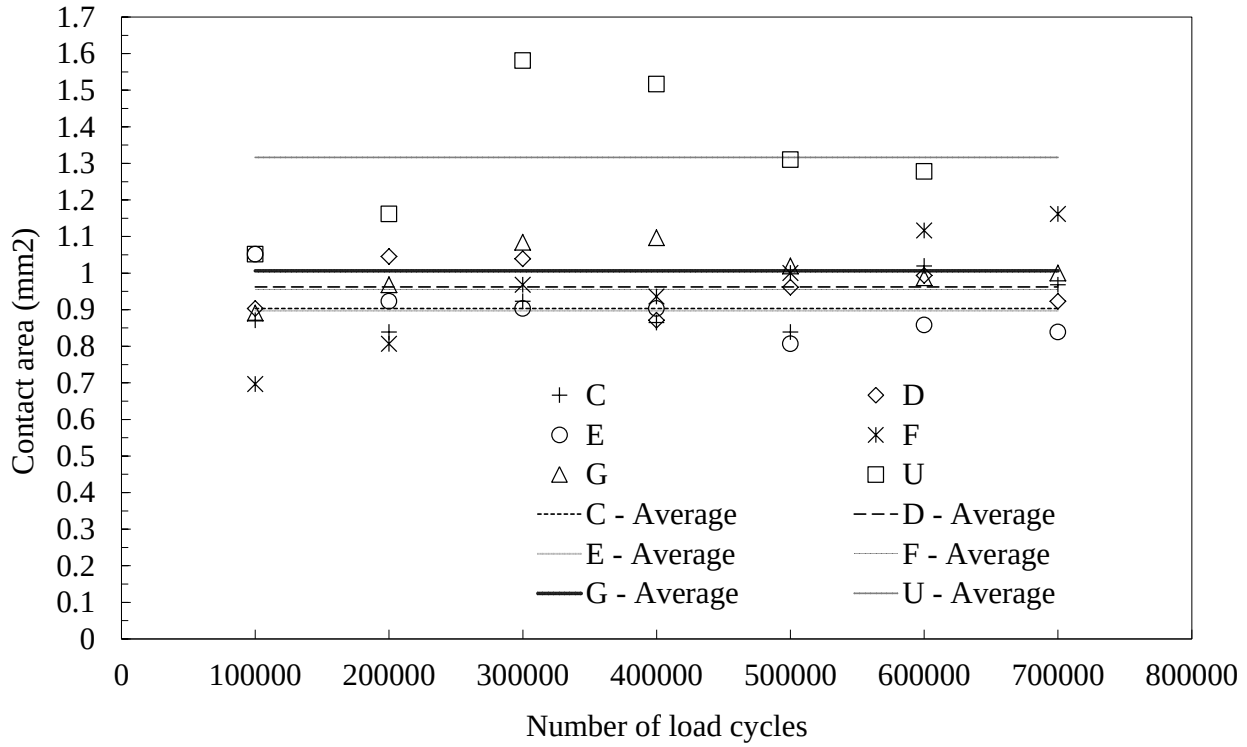

Figure 4. Contact area versus number of fatigue cycles for the different materials analyzed in this study.

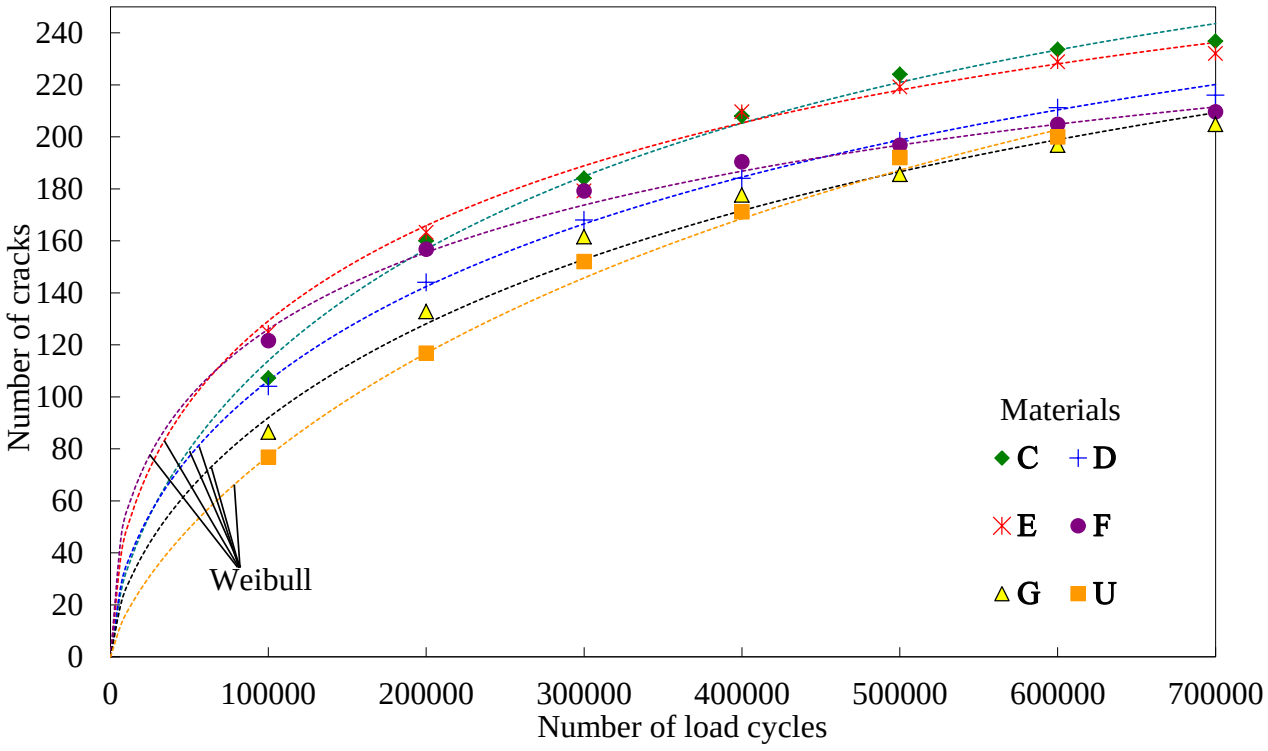

Figure 5. Effect of fatigue cycles on average crack density of wheel

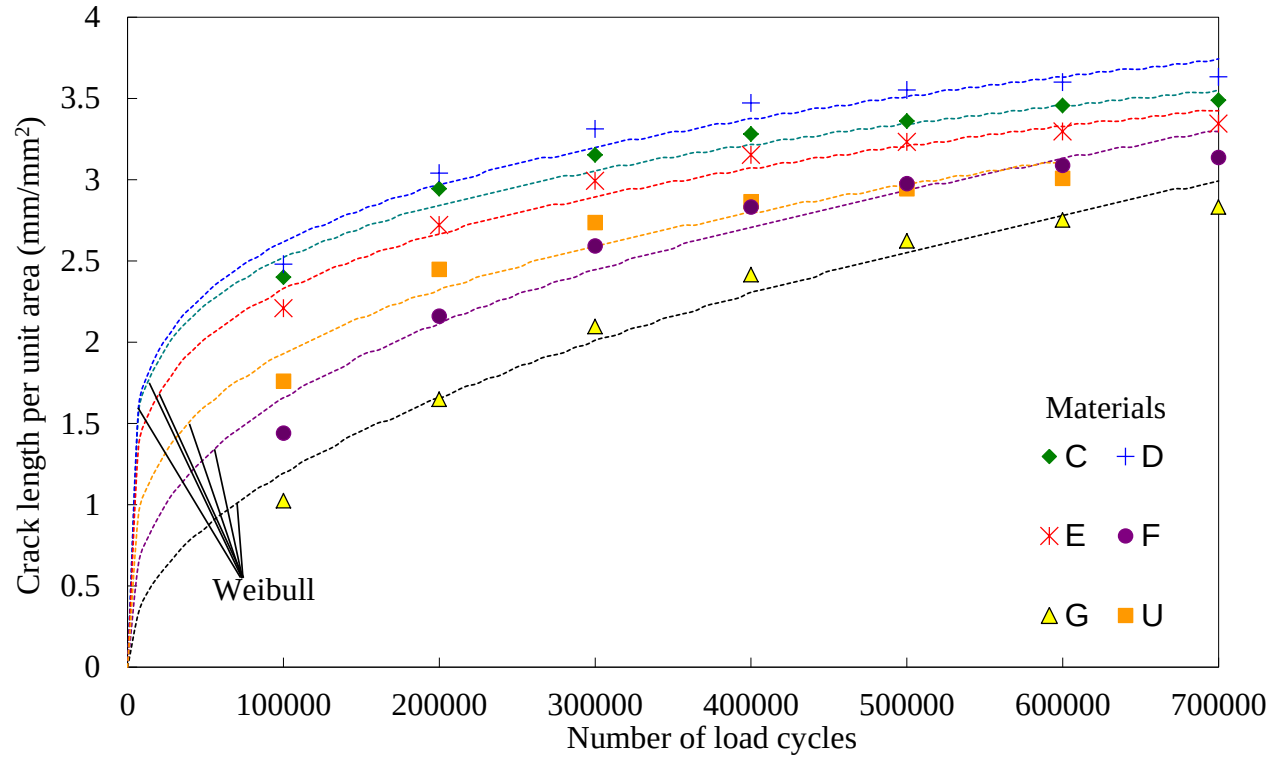

Figure 6. Effect of fatigue cycles on surface crack length density

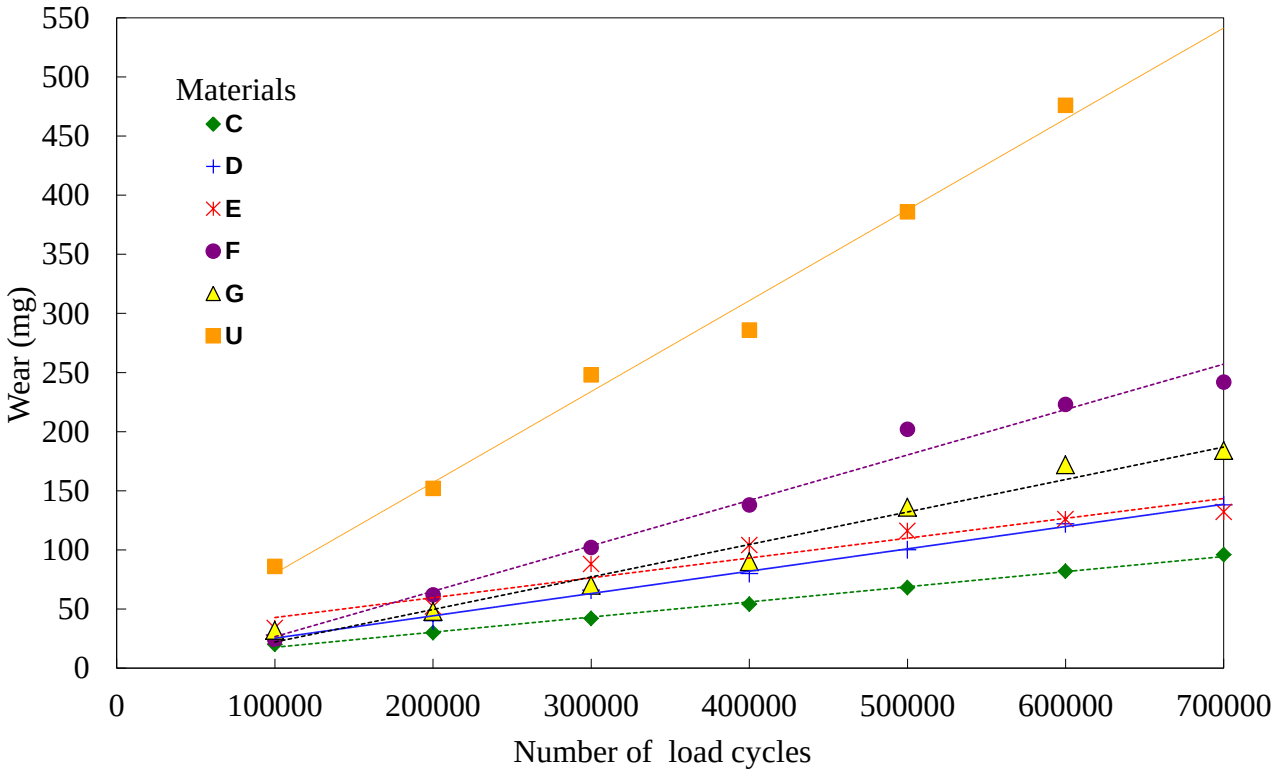

Figure 7. Effect of fatigue cycles on wheel wear

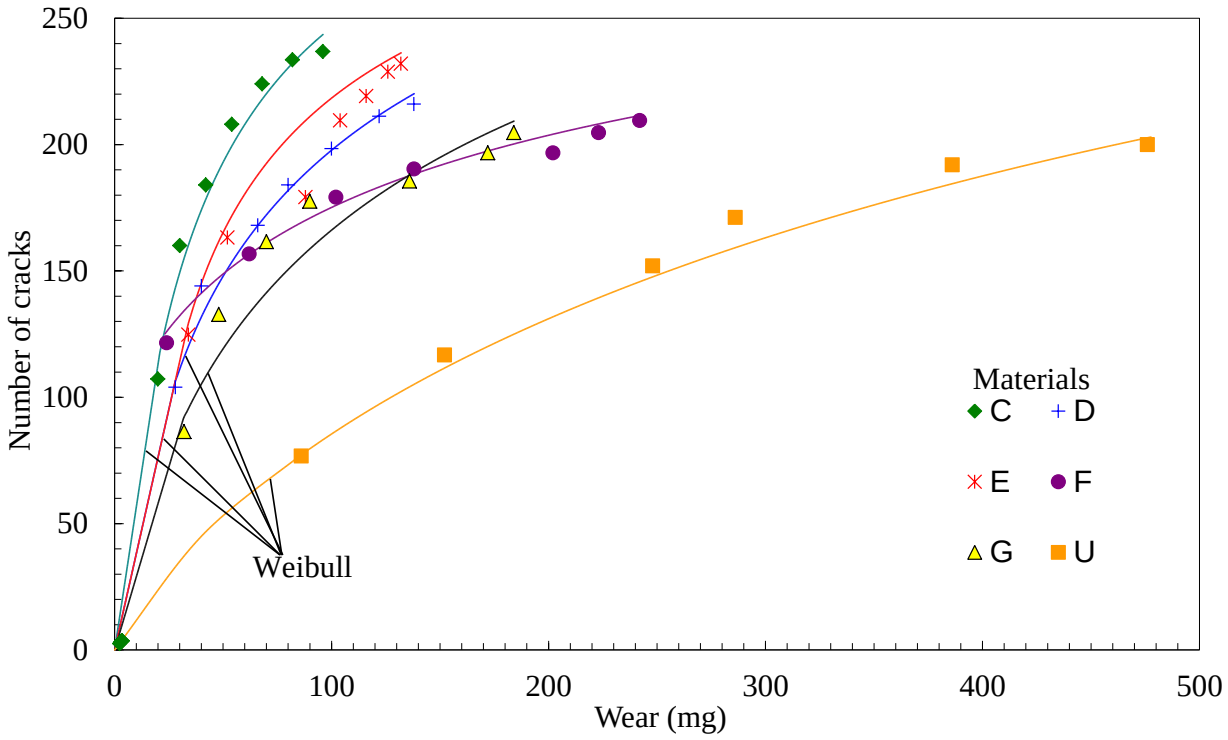

Figure 8. Effect of wear on the number of cracks

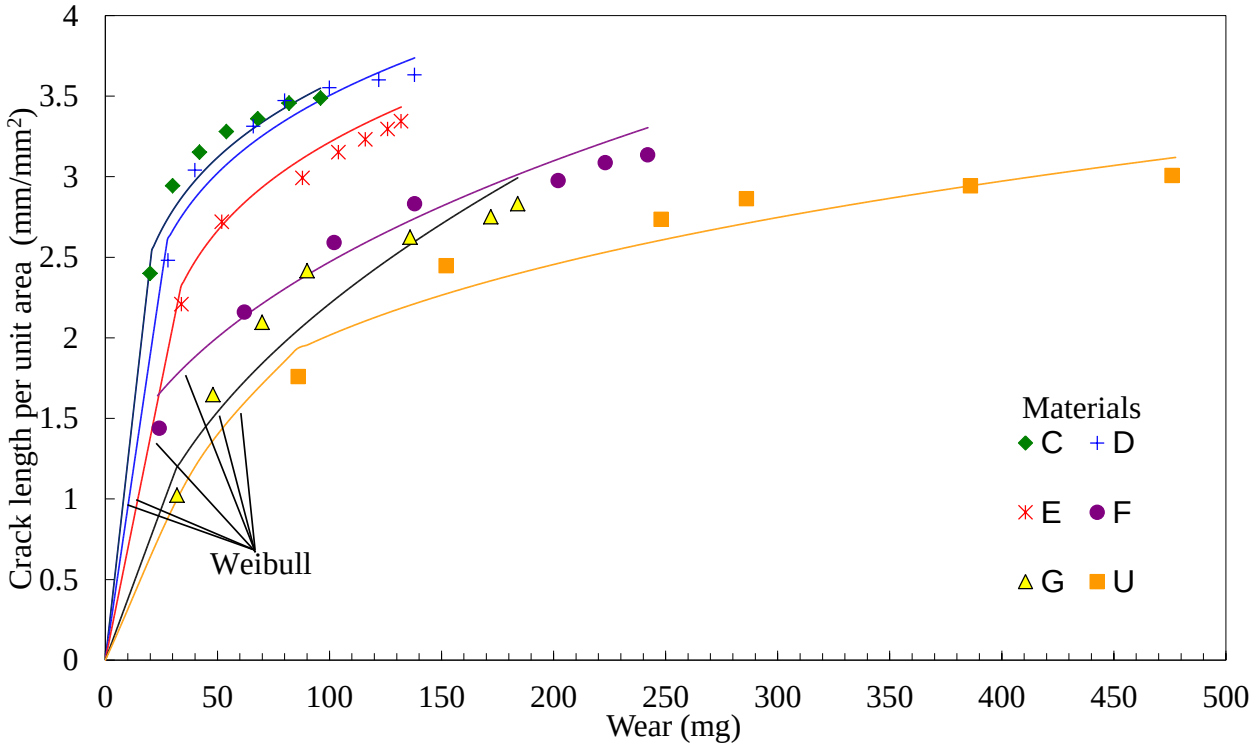

Figure 9. Effect of wear on crack length

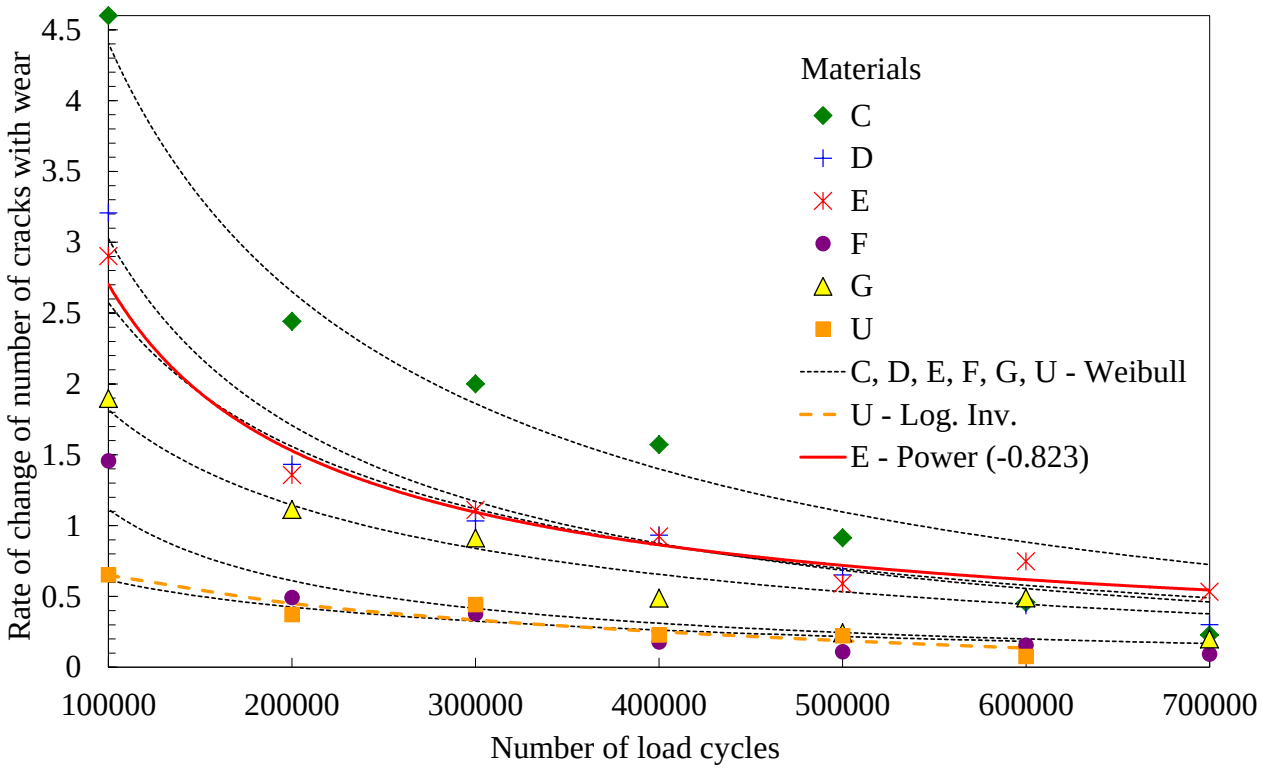

Figure 10. Rate of change of number of cracks with wear ($\partial N_{CR}/\partial W$) as fatigue cycles progress.

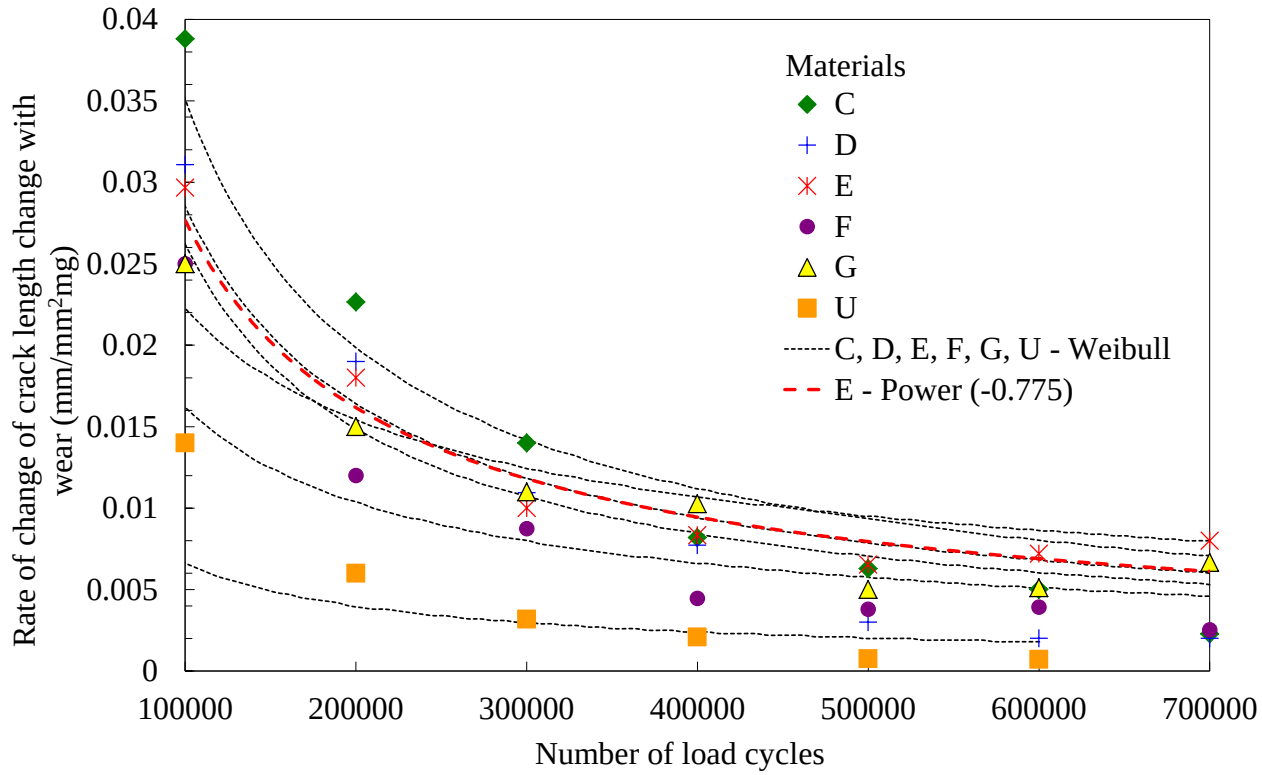

Figure 11. Rate of change of average crack length with wear ($\partial L_A/\partial W$) as fatigue cycles progress.

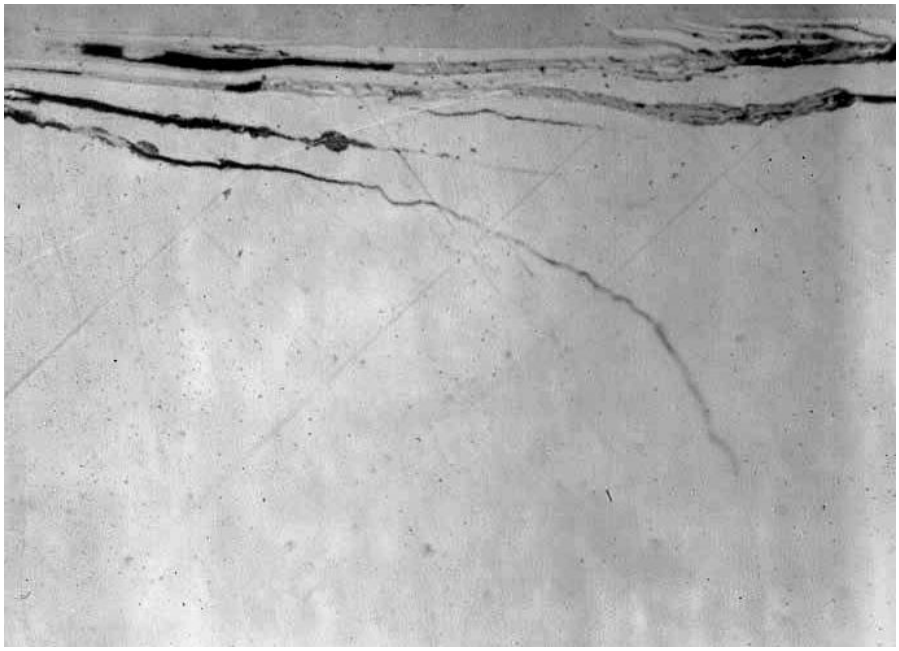

Figure 12. C-Simulated wheel. Cross section parallel to track. N=$8 \cdot 10^5$ cycles. Optical microscope with 400X magnification. Refer to Figure 13 for the quantification of the crack size (depth and length).

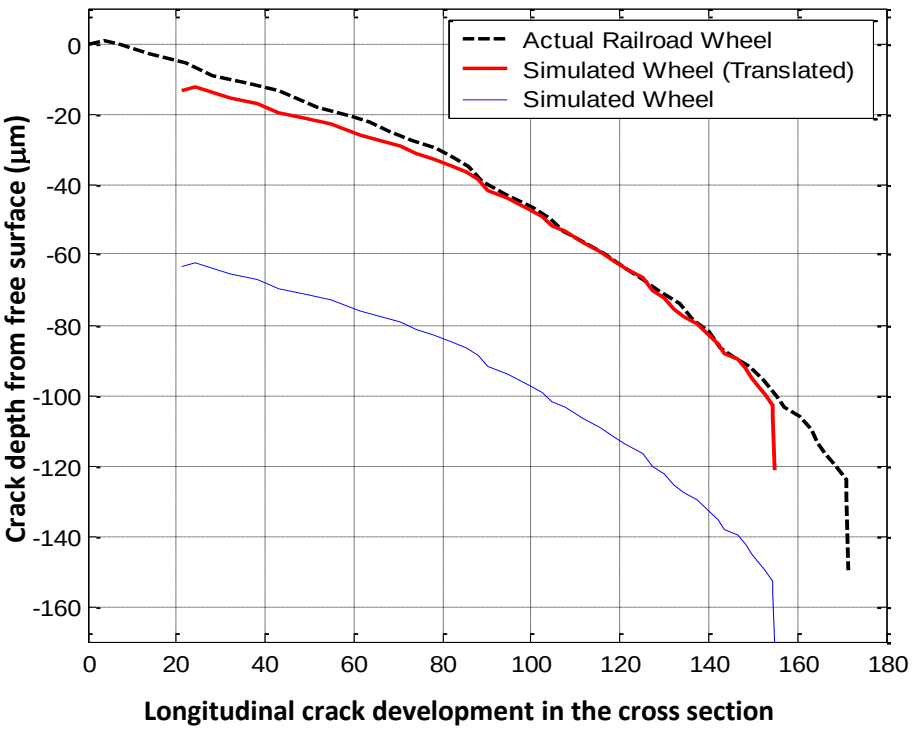

Figure 13. Comparison of real crack pattern and crack pattern generated in the experiments; the y-axis represents the depth of the crack starting from the free surface, while the x-axis represent the longitudinal crack development of the crack starting from the initiation site. Refer to Fig.12 for the real image.

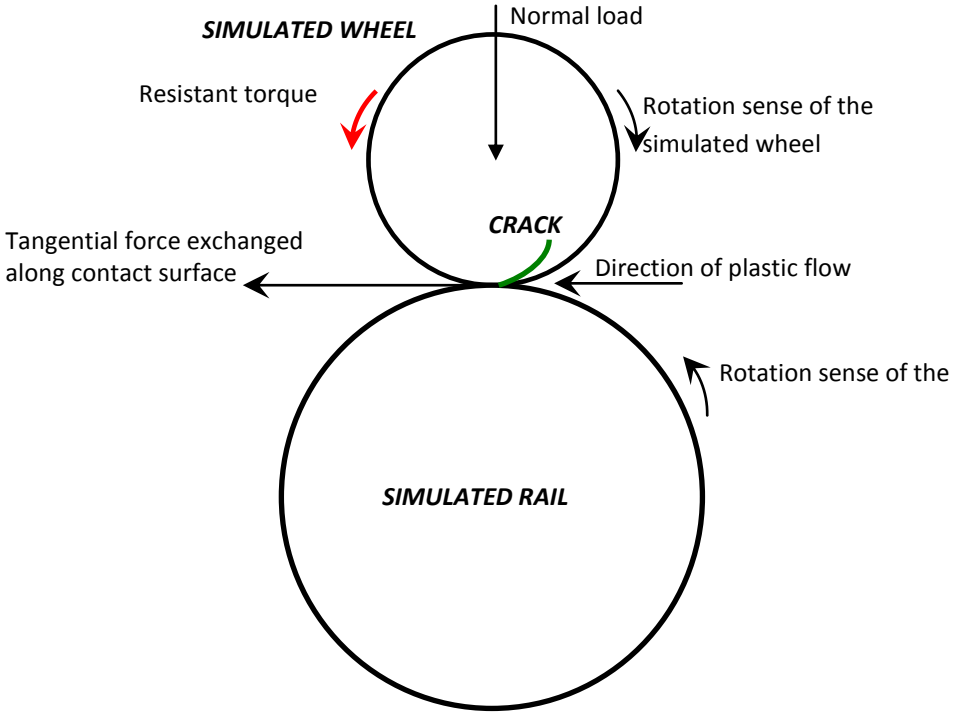

Figure 14. Schematic of rolling contact between wheel and rail

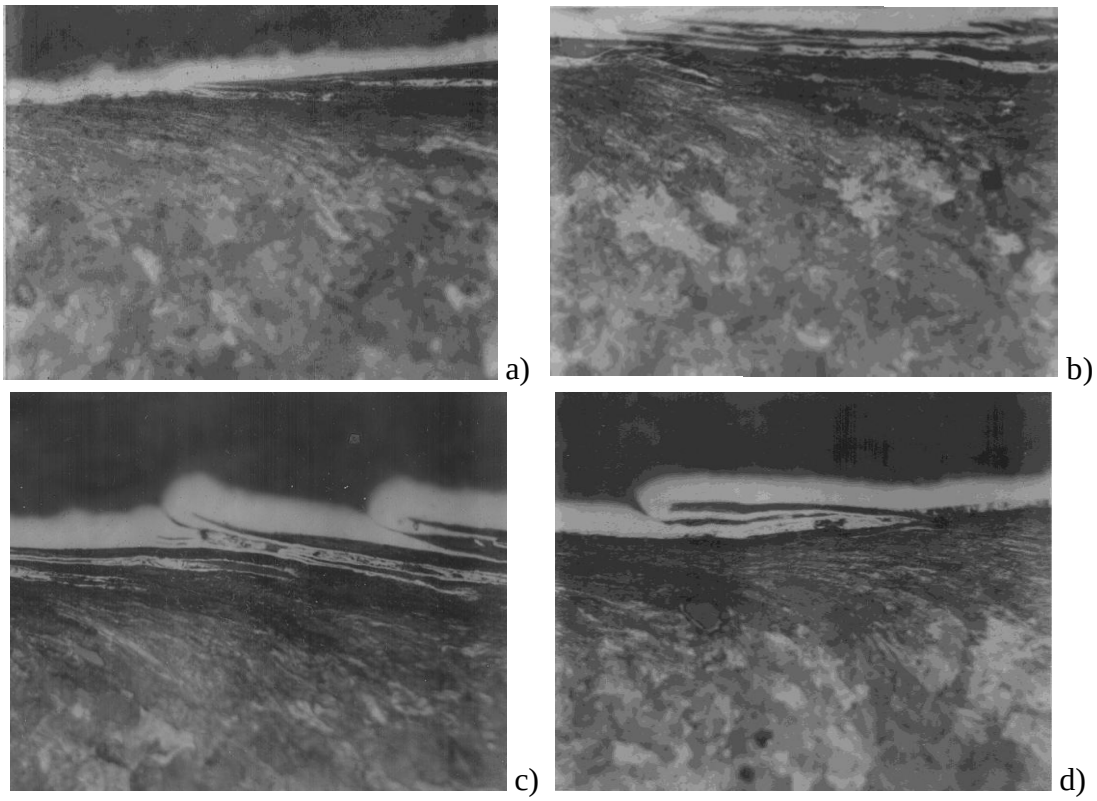

Figure 15. C-Simulated wheel. Cross sections parallel to track. N=$8 \cdot 10^5$ cycles. 3% Nital etchant. Optical microscope with 400X magnification.

Figure 16. D-Simulated wheel. Cross sections parallel to track. $N=8 \cdot 10^5$ cycles. 3% Nital etchant. SEM with 1000X magnification.

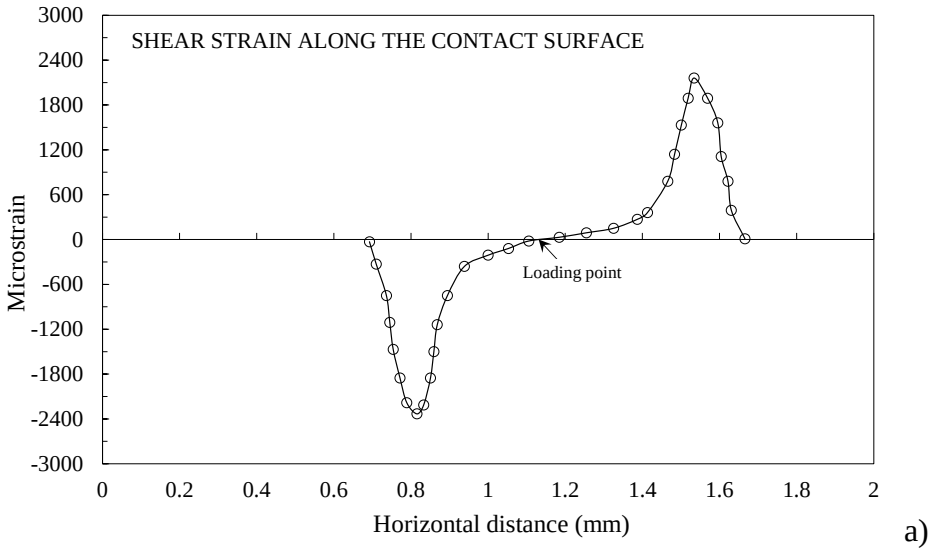

a)

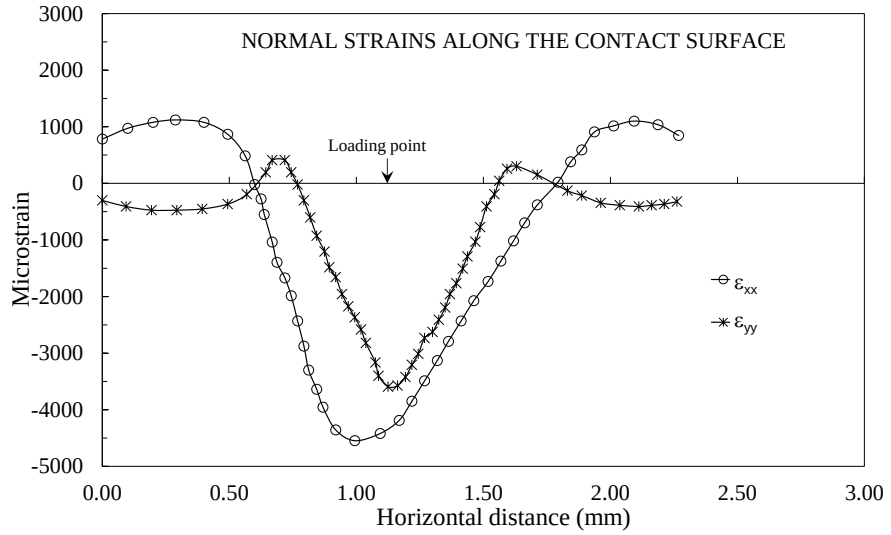

b)

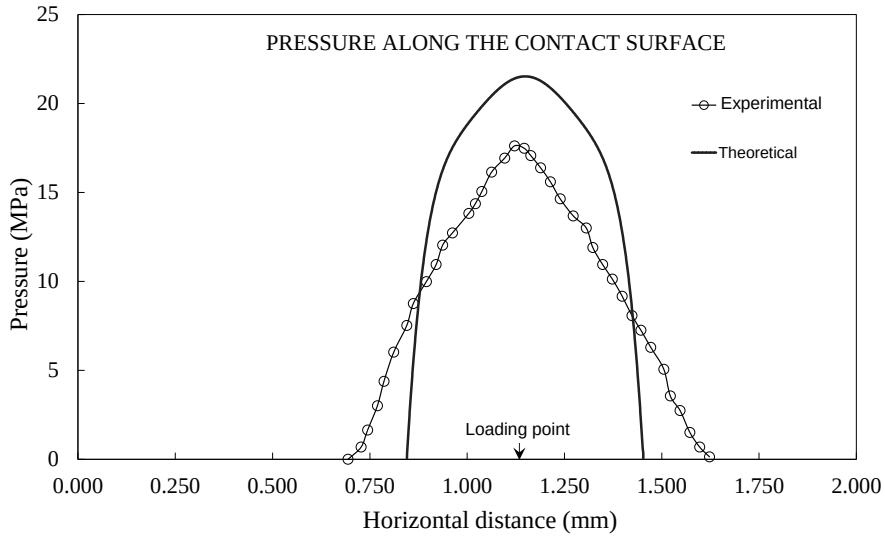

c)

Figure 17. 3D distribution of contact strain and stress (b-d) for a spherical ball against a simulated infinite plane (taken from [25,26])

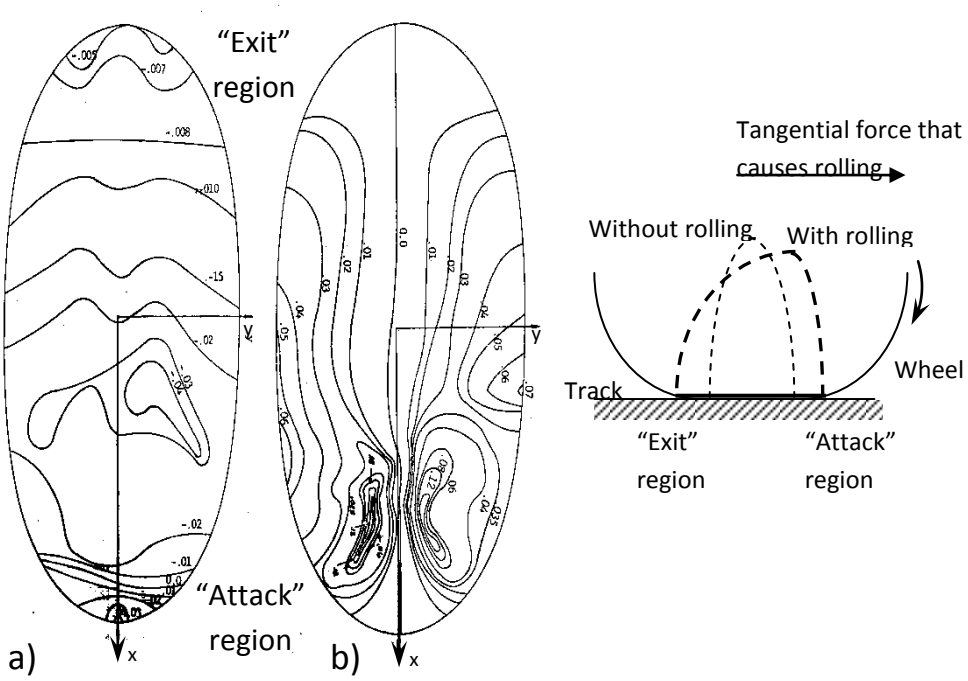

Figure 18. Contours of constant residual strain on wheel contact area taken from [27]: a) ε_x; b) ε_y. Pressure peaks move towards the "attack" region where contact initiates

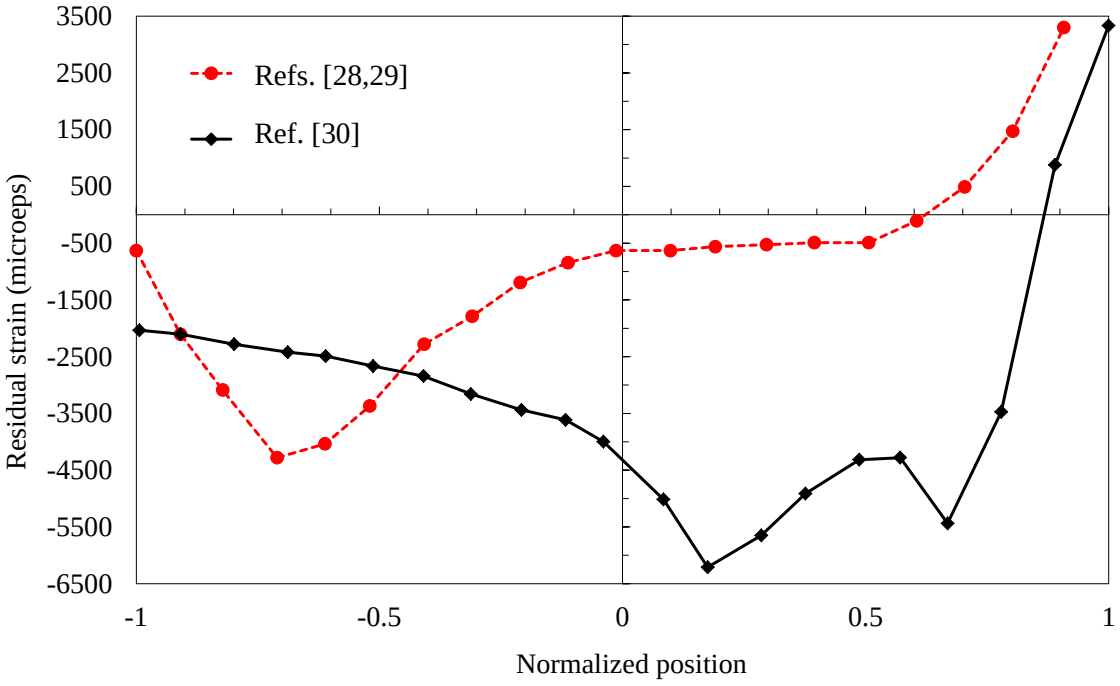

Figure 19. Longitudinal residual strains in the contact area measured with moiré techniques (taken from [28-30])

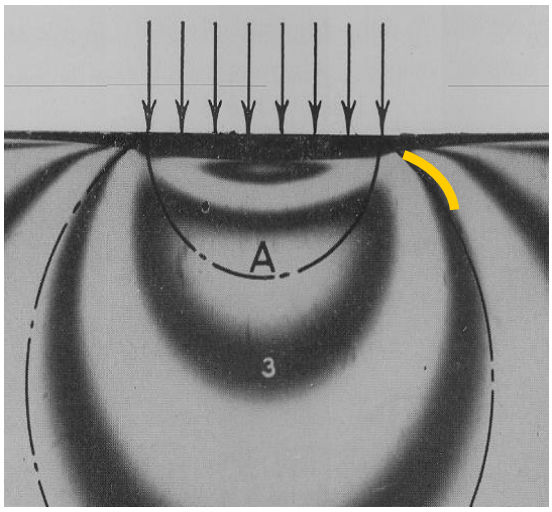

Figure 20. Photoelastic pattern of an infinite plate under an uniform load [31]

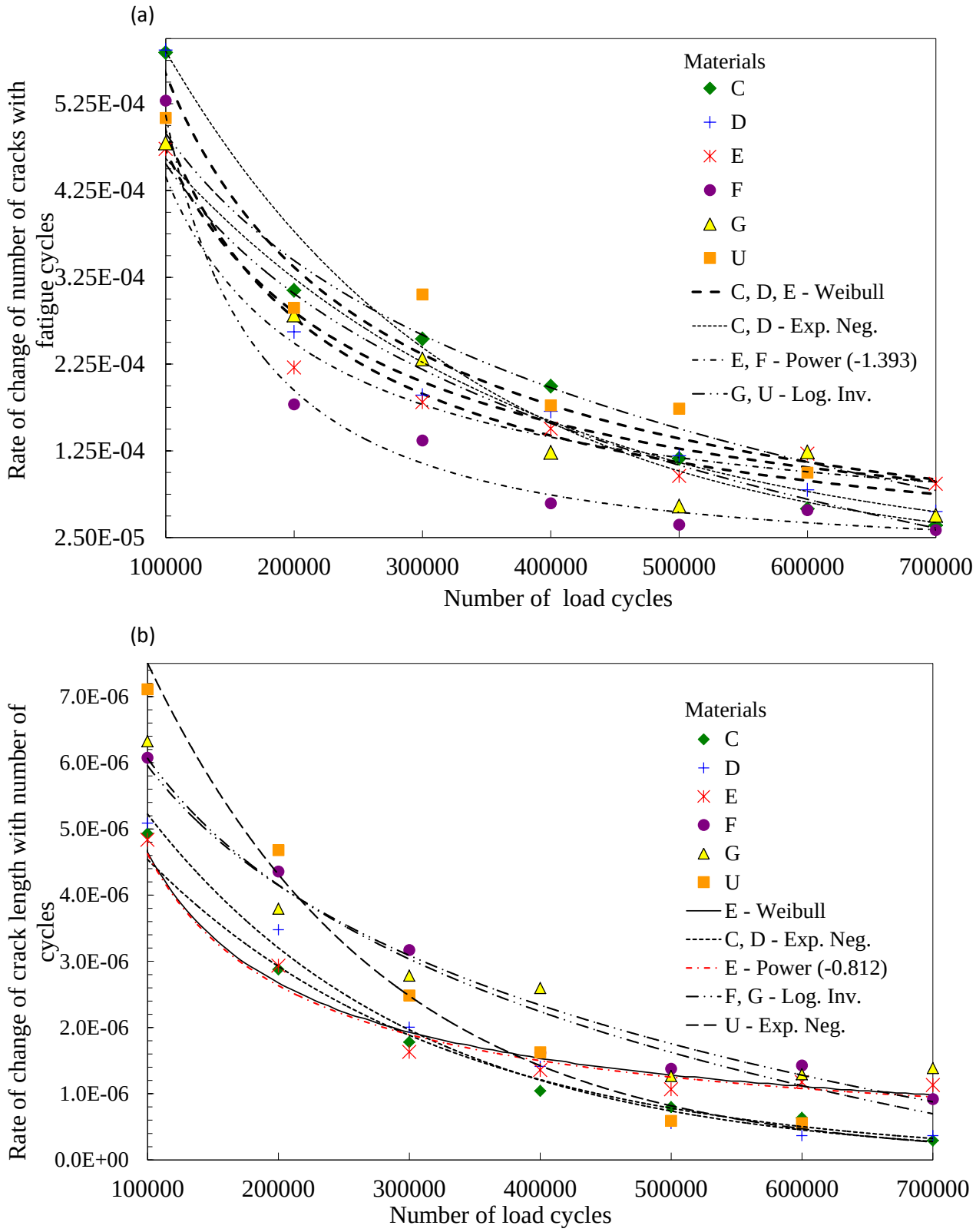

Figure 21. Rate of change of number of cracks ($\partial N_{CR}/\partial N$) (a) and crack length ($\partial L_A/\partial N$) (b) with cycles as fatigue progresses. Best fit models are plotted for all materials; Weibull fits are plotted only if the average error with respect to experimental data is less than 15%.

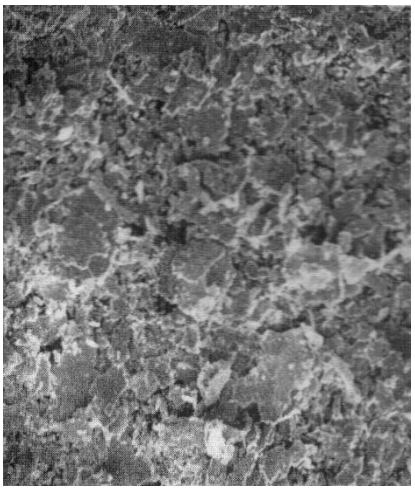 a) 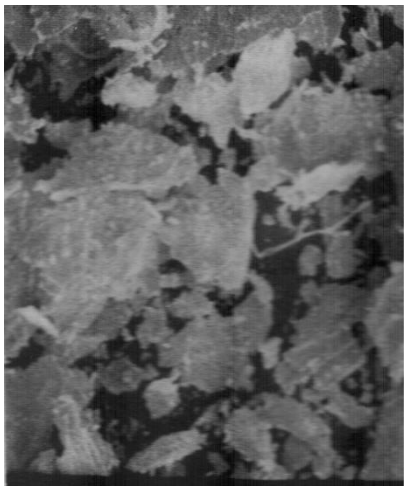 b)

Figure 22. SEM pictures (100X) of wear particles from test facility (a) and actual railroad (b)

EXPERIMENTAL EVALUATION OF ROLLING CONTACT FATIGUE IN RAILROAD WHEELS

C.A. Sciammarella[1], R.J.S. Chen[1], P. Gallo[2,3*], F. Berto[3,4], L. Lamberti[5]

[1] *Illinois Institute of Technology, Dept. Mechanical, Materials and Aerospace Engineering, 10 SW 32nd St, 60616 CHICAGO USA*

[2] *Aalto University, Department of Mechanical Engineering, Marine Technology, Puumiehenkuja 5A, 02150 Espoo, Finland*

[3] *University of Padova, Department of Management and Engineering, Stradella San Nicola 3, 36100 Vicenza, Italy*

[4] *NTNU, Department of Engineering Design and Materials, Richard Birkelands vei 2b, 7491 Trondheim, Norway*

[5] *Politecnico di Bari, Dipartimento di Meccanica, Matematica e Management, Viale Japigia 182, 70126 – BARI, ITALY*

sciammarella@iit.edu, pasquale.gallo@aalto.fi, filippo.berto@unipd.it, luciano.lamberti@poliba.it

Abstract

Surface damage in railroad wheels is a very complex phenomenon and the contact fatigue plays a fundamental role in the damage process. In the case of railroad wheels the actual fracture process is quite different from the conventional idea of fracture in a load bearing structural component. The cracks that are generated by contact fatigue are not the source of actual wheels cracking but lead to the damaging phenomenon called shelling which implies separation of chunks of material from the surface. Shelling is mainly due to the presence of a fluid in the contact area, which penetrates in the fatigue cracks and causes a crack propagation leading to the separation of a portion of the wheel surface. A basic starting point to analyze this phenomenon is to study the crack development in the contact surface and to evaluate the behavior of different types of steels used for wheels manufacturing. However, the challenge to obtain a reliable similitude between laboratory and real conditions is far from straightforward.

The present paper illustrates an experimental approach for rolling contact fatigue and shelling evaluation based on the possibility of simulating, in the laboratory, boundary conditions that can be scaled to the actual railroad, thus providing a realistic evaluation of the contact fatigue life of different steels.

Key words: Rolling contact fatigue; crack propagation; fatigue; rail vehicles; railway engineering;

***Corresponding author:** pasquale.gallo@aalto.fi

1. INTRODUCTION

Wheel-rail interface and, more in general, the rolling fatigue, has been a really attractive research topic for several years, simply consider that the first stretch of a railway line with locomotives and regular traffic was opened in England in 1825. In that period, massive railway projects were launched in many countries all around the world [1], such as in Sweden and Norway. The improvement of this complex and fascinating machine has never reached a break, leading today to superlative examples of cutting-edge technology, e.g. Japanese Shinkasen and French TGV that can easily reach speed higher than 300 km/h. The design of these machines is anything but easy and different aspects still result critical nowadays. One of them is the wheel-rail contacts. For the wheel-rail interface, the pioneering scientific breakthroughs occurred in the 1880s. Worth mentioning Heinrich Hertz, who proposes a theory of elastic contact that found soon application in railway engineering, followed by other researchers, and August Wöhler, in the 1850s, who studied the fatigue phenomenon in the case of railway axes. The fundamental theory of rolling contact fatigue instead was published in 1947 by Gustaf Lundberg and Arvid Palmgren. Their application was rolling bearings [2].

From those pioneering works, higher speeds and greater axle loads are creating more demanding operating conditions for the wheel-rail interface, while in parallel, development of advanced numerical models and computer based simulations, led to a refined adhesion control of traction and braking, with optimization of the wheel-rail interface followed by new and different problems [1]. In the contact zone, indeed, several undesired phenomena may occur: high vertical contact forces, but also lateral and longitudinal forces, induce stresses that may cause material yielding and fatigue; rolling contact forces combined with friction induce wear; traction and breaking may lead to wheel sliding resulting in rail burns and wheel fault, unfavorable material phase transformations, and thermal cracks [1]. Different phenomena to be faced with involve different research fields: contact mechanics, material mechanics, tribology and dynamics, railway noise, vibration, rolling contact fatigue and fracture mechanics are examples of the most “traditional fields”. Among them, rolling contact fatigue (RCF) manifests itself in crack formation and crack growth in the material close to, or at, the wheel-rail interface. Crack initiation can occur in the surface, normally due to severe plasticization, and at a subsurface level (from microstructural defect). The study of RCF, through the fracture mechanics, is far from straightforward. In fact, several complicating factors are involved, e.g. complex states of stress and strain, crack face friction and anisotropic material, fluid entrapment in the crack. It is well known that considerable studies on RCF in rail have been conducted, but some lack in our knowledge still exist, for example: crack initiation and wear, crack propagation by contact

stresses, crack propagation controlled by bending stresses. It should also be mentioned the challenge to obtain a reliable similitude between laboratory and real conditions.

The complex phenomena presented in the introduction have been considered by different authors also in the recent literature, briefly recalled below.

In the work by Kondo at al. [3], a study on the shelling phenomenon affecting Shinkansen trains was presented. In that original work, discussion of the causes and applied counter measures of shelling were presented. Despite the deep analyses and discussion of the results, the mechanics of shell formation was not well understood.

An interesting work regarding rail rolling contact fatigue was presented in Ref. [4]. The paper summarized the state of the art and a review of the research program of the "European Rail Research Institute". Laboratory experiments were conducted on small scale rotating test pieces and on full scale rolling wheel on rail tests. Despite several difficulties experienced, RCF damage was produced but laboratory testing to simulate service rolling contact conditions remains problematic.

A comprehensive review was recently presented by Sadeghi et al. [5] regarding RCF of bearings. In that paper, some of the most widely used RCF models were reviewed and discussed, and their limitations addressed. The paper also presented a new model developed by the authors considering a non-homogeneous microstructure of randomly shaped, sized and oriented grains.

An investigation of the effect of train curving on wear and contact stresses of wheel and rail was conducted in [6]. The authors focused on the stresses due to the wheel/rail contact, on the wear and on the effect of railway vehicle curving. A sophisticated numerical method was presented and it was found that the material wear volume per length along the rail running surface had a tendency to grow. The wear changes the profiles of the wheel and the rail, and leads to the serious problems, but, the wear can efficiently eliminate small cracks on the rail running surface, and suppress the growth of the cracks. Based on that principle, railway companies scientifically grind the rails in service to relax the contact stresses, eliminate and reduce the rolling contact fatigue of the rails.

RCF crack growth was analyzed in detail by Zhong et al. [7] in terms of chemical composition, mechanical performance and microstructure. The crack propagation in rails under RCF is of vital importance for the railway industry. Some authors tried in the past to develop tools for crack growth prediction. Numerical simulations of crack growth in rails were proposed in Ref. [8], focusing on short surface head check like cracks, often observed at the rail gauge corner. The result suggested that anisotropic effects from the highly deformed surface layer may need to be included in order to simulate head check growth in rails accurately.

Some attempts to model rate of wear and RCF on the wheel were also made recently [9,10]. For example in Ref. [10], the development of a damage model to predict the deterioration rates of the wheel tread considering wear and RCF was presented. The damage model was previously validated using observation data on different vehicles. Despite the good results, further analysis are required to understand the influence of parameters involved on wheel damage (e.g. traction and braking, wheel slide protection systems efficiency).

In order to study the effect of tangential force on wear and rolling contact fatigue behaviors of wheel material, experimental tests were conducted by He et al. [11] recently. Surface damage behavior observations permitted to assess the influence of tangential force on RCF and wear.

Interactions between RCF and wear of rails were recently analyzed by Seo et al. [12]. The test specimens did not have the same dimensions of the real components, but were taken from the rim of a wheel and the head of the rail. To reproduce material surface conditions of a real-sized wheel and rail using the small-sized specimens, a series of heat treatment processes were applied. Also the surface roughness of the rail was reproduced.

The competitive relationship and interaction within rolling contact fatigue damage and wear was also considered and presented by different authors, e.g. see Ref. [13-15]. An attempt to realize experimental tests that represent the real working conditions of wheel-rail contact was made by Mazzù et al. [16]. RCF tests were carried out on cylindrical discs with diameter of 60 mm and 15 mm thick. Other interesting papers have been presented by the same authors regarding numerical approaches, models, and failure assessment of rolling contact fatigue and wear [17–20].

The previous discussion demonstrates that rolling contact fatigue of railroad wheels and the related experimental simulations still represent a fundamental and attractive research topic. In view of this, the present study aims to investigate the reasons for heavy damage of truck wheels in a particular railroad service region where the tonnage is steadily increased (mean axle load 37 tons). Another objective is to properly evaluate a variety of steels and thermal treatments in order to improve fatigue life of wheels. Rolling contact fatigue was evidenced by the formation of shallow shells. However, it was not clear the mechanism of the crack formation and propagation. Preliminary analysis of early damage of wheel's surface showed parallel cracks at very regular intervals perpendicular to the rolling direction (about 1 mm apart). A typical cross-section of the cracks parallel to the rolling direction (see Figure 1) shows a crack propagating initially in mode II, and finally approaching mode I until the crack propagation is stopped by a reduction of the stress. From these observations it was concluded that the damage of the wheels was not the result

of the typical contact stresses damage caused by rolling, since cracks seem to start at the surface and not at the level where the shear stresses are maximum (as it occurs in roller bearings).

2. APPARATUS AND EXPERIMENTAL DETAILS

2.1 Experimental set-up

The experimental set up was realized in order to investigate the rail-wheel RCF problem and provide the capability of material evaluation, reproducing in the most faithful way the real conditions affecting real wheels. It must be pointed out that, because of the vast complexity of the problem under analysis, costs restraint effective research and represent an important factor to be considered in experimental determinations.

The actual distribution of contact stresses is very complex and statistical in nature. The characteristics of the wheel that have an important effect on the stress field are: shape design (this is a trade-off between steering capabilities and fatigue), wear requirements (these variables define the stresses distribution), adhesion creep characteristics of wheel material, development of residual stresses due to plastic work-hardening, presence of thermal stresses generated during braking. These characteristics are quite complex and depend on a large number of variables. Wheel and rail are envelopes of each other and their relative profiles are continuously changed by wear and by resurfacing that is part of the maintenance work. In order to simplify the problem, a wheel-rail simulation device was designed and built in this study. The testing apparatus, shown in Figure 2, includes the following components:

- Small wheel (simulated railroad wheel) riding on a larger wheel (simulated rail);
- DC motor coupled with a reducer;
- Continuous speed controller;
- Belt transmission system;
- Magnetic pick-ups and electronic counter;
- Pneumatic brake;
- Brake control unit;
- Torque measuring device;
- Steam supply unit;
- Digital counter.

The wheels are shown in Figure 3. The simulated wheel may be represented by a cylindrical surface, while the simulated rail is represented by a circular cross section. The wheel was accurately designed in order to reproduce elastic Hertzian contact normal stress distribution, derived from a 100 ton train car. The assumption of the Hertzian theory is a well-established

procedure when dealing with rail-wheel contact problems as shown in the references given in the introduction. The normal load was applied to the small wheel by a cantilevered gravity loading system through a fork holding the small wheel bearings.

The rolling speed of the wheels was monitored through the continuous speed controller.

Magnetic pick-ups (number 6 in Figure 2) served to measure the individual rotating velocities of the wheels and the electrical outputs were fed to an electronic counter that yielded the individual speeds and the speed's ratio with four significant figures. A friction force was applied by braking the simulated wheel with a pneumatic brake. The applied torque was measured by a strain-gage torque sensor. The braking torque was calibrated as a function of the applied pressure.

2.2 Important aspects of the set-up design and performance

The experimental set-up was designed on the basis of previous experience accumulated in performing tests with larger facilities. The idea was to simulate the real operating conditions as closest as possible within reasonable limits. The basic starting point is suggested by the theory of similitude, getting the same initial Hertz contact stresses with the same materials used in the actual wheels and rails. The contact between wheel and rail changes drastically as the rolling takes place [21–23]. The wear and the plastic deformations change the initial Hertz ellipse to an almost rectangular area of contact. The width of the contact area is determined by the profile radius and the wear rate. The width increases as the wheel rolls until a state of equilibrium is reached and changes in the contact area become minimal.

The effect of the different variables such as adhesion, creep, normal, tangential loads, roughness has been analyzed and found to be consistent with previous observations conducted in the past [24]. One important conclusion is that the product of the area times the creep remains a constant for a given value of the normal load P, friction coefficient μ and critical coefficient μ_c, where this is the maximum coefficient of friction that is used to derive a dimensionless creep curve. As a consequence of this observation, measurements were carried out after a fixed number of cycles required for a stabilization of the contact area. From that point it was checked that the contact area remained constant within a certain standard deviation depending on the particular material used in the simulated wheel. The rail material instead was not varied. In freight railroad track a wheel passes over a particular portion of the track within a period of time. During this time the rail surface oxidizes and the rust formed prevents a direct metal to metal contact between wheel and rail. In the laboratory tests, experimental conditions prevent formation of dust thus leading to the possibility of direct metal-to-metal contact generating phenomena such as cold pressure welding, vibration and slip. In order to avoid all these problems it was injected a

small quantity of dry vapor, avoiding undesirable phenomena like water penetration in the surface formed crack.

2.3 Testing procedure

Six different materials have been considered and two wheels for each material have been tested according to the procedure described in the previous section. They are designated as C, D, E, F, G, U. Summarizing test conditions:

- Constant normal load P = 242.4 N;
- Same tangential load T = 0.2 x 242.4 = 48.48 N;
- Same geometries of simulated wheels and rails (see Figure 3);
- Same environment;
- Same roughness (0.0003 CLA).

The following data were collected every 100,000 cycles:

1) *Contact area*.
2) *Crack density*. The crack density was determined by counting cracks in the observed regions. For each material two wheels were studied and 20 pictures were taken. The images were taken with 50X magnification. A microscope with a 10X objective and numerical aperture 0.25 was utilized. The objective has a resolution of 1 μm. An 5X ocular was used and a camera with an additional magnification of 4X was used to get micro-photographies of size 0.4775 mm x 0.365 mm. To standardize the test, 10 μm was considered the crack initiation length. With this procedure, ensemble average of crack density was calculated every 100,000 cycles.
3) *Crack length*. The formed cracks are curved surfaces which can roughly considered as elliptical. The measured crack length is therefore only the crack propagation on the surface.

Once the test stopped (every 100,000 cyles), the following operations were performed on the wheel and rail:

1) The wheels were removed; the sense of rotation of the small wheel was saved using a marking arrow.
2) The simulated wheel (SW) was cleaned with methanol and then in an ultrasonic bath.
3) The SW was weighted in an electronic balance with an accuracy of 0.0001 g.
4) The SW was mounted in a Vernier-rotating stand for observation with a microscope. The track surface was observed and 10 micrographs were taken 36^{o} apart.
5) The simulated rail was resurfaced to keep the original radius and polished to the initial finishes.

The experiments were performed as described for 700,000 cycles. In addition to the above tests for crack analysis, more 100,000 cycles were added for pitting damage investigation. In this case, the vapor was replaced by water drops to induce pitting due to the water pressure. The water test was conducted on wheels that have already been cracked. In the actual wheels and rails the presence of liquids influences the already cracked wheels; the liquid is an additional factor that adds a load to the existing crack.

After 800,000 cycles, the small wheel was subjected to metallographic analysis using cross-sections parallel to the rolling direction. A 3% Nital (alcohol and nitric acid) solution was used to etch the specimens. Regarding the pitting tests, SEM images of the specimens were taken.

2.4 Material properties

Six high strength steels for rail constructions were tested in the experiments, and are here classified as a function of their hardness. In detail: the initial C-Rockwell hardness, the Knoop micro-hardness outside the track area after the tests (HK-Out) and the Knoop micro-hardness inside the track area after test (HK-In) are given in Table 1. Materials C, D, E and G are harder than materials F and U. Materials and specimens were provided by manufacturers as the representative elements that they use in the manufacture of the corresponding parts.

As far as it concerns changes experienced by the material during testing the following measurements were taken:

1) The rims of the simulated wheel and the simulated track were subjected to C-Rockwell measurements.
2) All the wheels were subjected to micro-hardness tests, both in the contact region and outside the contact region.

3. TECHNIQUES FOR DATA ACQUISITION PROCESS

The accuracy and reliability of the presented results depend in large extent on the techniques involved in the data acquisition process. Some of the techniques involved in this paper were developed and improved at the Illinois Institute of Technology (Chicago, USA) and are presented in the following subsections in detail.

3.1 Measurement of the contact area between rail and wheels

This task was accomplished by using a 4 mil (i.e. 102 μm) replicating transparent tape placed between simulated rail and wheel. The replica technique is based on a similitude law between the replica left on the tape and the actual contact area as predicted by the Hertz theory. This

technique has been verified in the measurement of the contact areas in reduced scale models as well as in actual railroad wheels.

3.2 Measurement of the rolling speeds and relative sliding.

The speed of rotation was measured with magnetic pick-ups with a resolution of 1/144 of a revolution. The following equation has been adopted:

$$\xi = 1 - \frac{R_S N_S}{R_B N_B} \tag{1}$$

where ξ is the longitudinal creep; R and N, respectively, indicate the radius and the number of revolutions of the wheels per unit time; the subscripts S and B indicate the small wheel (simulated wheel) and big wheel (simulated rail), respectively. Study of the accuracy of the measurement of the creep can be found in [24].

3.3 Measurement of the coefficient of friction.

The coefficient of friction was determined from the following relationship:

$$\mu = \frac{T}{P} \tag{2}$$

where P is the normal force and T is the tangential force. A torque meter based on strain-gages senses the torque applied by the brake. This torque is directly proportional to the coefficient of friction between the two wheels as long as slip between the two wheels does not occur. This condition can be verified easily by observing the velocity counter. A calibration was performed by applying a known torque. The following equilibrium equation can be written,

$$T \cdot R_S = Q \cdot L_B \tag{3}$$

In this equation, T is the tangential force applied to the small wheel surface, R_S is the radius of the small wheel, Q the force that multiplied by the lever arm L_B gives the value of applied torque. Since $T = \mu P$, where μ is the coefficient of friction and P is the applied normal force, it follows from Eq. (3),

$$\mu = \frac{L_B \cdot Q}{R_S \cdot N} \tag{4}$$

Calibration was performed and thus μ becomes a function of the reading of the strain-gage bridge. Being available the relationship within the friction coefficient and the strain-gage bridge, an indirect measurement of the coefficient has been made possible during the test.

In detail, first a desired value of the friction coefficient has been imposed a priori, that is μ=0.2. In turn, the corresponding value of the strain indicator, that is 272.5 με, has been determined. Knowing the target of strain indicator value that assures the desired friction coefficient, during the experimental testing the value reported by the strain indicator has been checked to be as much close as possible to 272.5με, implying a controlled value of the friction coefficient close to 0.2. The variation of the measure has been also quantified in a 0.7% variation of the friction coefficient.

4. RESULTS

Because of the complexity of the CRF phenomena, different parameters were observed and related issues are briefly reported below for the sake of clarity. Extensive comments for these results are reported in a specific section later in the manuscript.

4.1 Contact area, ensemble average-crack density and surface average crack length

Figure 4 shows the measured contact area as a function of the number of cycles. Material U exhibited considerable dispersion while contact area remained close to the initial value for the other materials.

The ensemble average crack density of the different materials is plotted in Figure 5; trends show very little dispersion. Figure 6 shows the surface crack length density for the different materials. This quantity shows a regular progression with the number of cycles. Both data series were fitted by a 3-parameter Weibull distribution following Eq. (5):

$$F(N) = A\left(1 - e^{-CN^{\beta}}\right) \tag{5}$$

where N is the number of load cycles. The parameters A, C and β were determined by best-fitting experimental results: for that purpose, the Newton-Raphson method and a least square method were used. It appears that experimental data are very well fitted by the Weibull distribution: in fact, the average error made in the fitting operation ranges between 0.970% (material D) and 3.218% (material G) for the number of cracks, and between 2.274% (material C) and 5.024% (material F) for the crack length, respectively.

The crack density value is taken as an ensemble density distribution of events, the random formation of an individual crack due to the presence in the material of sources of damage initiation (weak links). At the end of the process there is a saturation in the number of cracks when the different cracks begin to interfere with each other and the process of crack creation and propagation slows down to a holt. A similar thing occurs with the density of crack length per unit area of the surface. The stabilization of the process means that the weak points at the surface neighborhood have been exhausted because of the prevailing stress level, and cracks have grown to dimensions such that they begin to shield one another. It is necessary an external factor, such as the presence of fluids on the track, to propagate a crack.

4.2 Wear

Wear is the loss or displacement of material from a contacting surface. Figure 7 shows the variation of the wear of wheels with respect to the number of cycles. It can be seen that wear increases linearly as load cycles progress: the correlation coefficient R^2 computed for linear fitting ranged between 0.934 (material F) and 0.997 (material G).

Considering the effect of wear on the crack initiation, there are two different active mechanisms of damage: surface damage due to the presence of very high stresses caused by local contact interferences of surface irregularities, and surface damage caused by global stress. The first produces the removal of superficial layers, while the latter generates deep penetrating cracks. The accurate observation of the tested surfaces showed the presence of both mechanisms.

The number of cracks as a function of the wear is depicted in Figure 8. This curve shows the effect of the hardness on the number of cracks generated. There are two mechanisms operating: crack generation and crack removal. The former predominates in harder materials. This is proven by Figure 8 which shows that for a given amount of wear the number of cracks is larger in the case of harder materials. Since wear linearly increases with the number of load cycles, Weibull distribution can precisely fit these data: the average error made in the fitting operation ranged between 0.989% (material D) and 3.23% (material G).

Figure 9 illustrates the effect of wear on crack length density L_A. This effect becomes less significant for softer materials while harder materials show larger values of crack length density. Weibull distribution fitted very well also these data: average error ranged between 2.30% (material C) and 5.38% (material F). This is another consequence of the linear relationship between wear and number of load cycles.

Figure 10 shows the variation of $\partial N_{CR}/\partial W$ (number of cracks/mg) with respect to the number of cycles: it can be seen that (i) such a rate decreases as fatigue loading progresses and (ii) softer materials present lower rates than harder materials. Weibull distributions fitting

experimental data also are plotted in the figure in order to have a homogeneous basis of comparison with the previous figures. It can be seen that the Weibull model fits experimental data far less accurately than in the case of number/average length of cracks vs. number of cycles/wear data (see Figures 5-6 and 8-9). In particular, the Weibull model was found: (i) to cover the entire range of load cycles considered in the experiments only for materials E and U (average errors between 8% and 11%), (ii) to be reliable only in the first half of fatigue life (i.e. until 300,000/500,000 cycles) for materials C, D and G (errors between 9% and 14%), (iii) not to be valid for material F. The data plotted in the figure were instead best fitted by inverse logarithmic (materials C, G and U), negative exponential (material D) and power functions (materials E and F); the corresponding correlation coefficients R^2 ranged between 0.887 and 0.979. The non-Weibull best fits for materials E and U are included in the plot: the former yields $R^2 = 0.951$ and crosses the corresponding Weibull fit at 400,000 cycles while the latter yields $R^2 = 0.887$ and is very close to the corresponding Weibull fit.

Figure 11 shows the variation of $\partial L_A/\partial W$ (mm/mm^{2}mg) with respect to the number of cycles. It can be seen that length change rate again decreases significantly with the number of revolutions. Weibull-based fitting is yet less accurate than before, mainly because $\partial L_A/\partial W$ is a rather small quantity which hence is more sensitive to numerical noise. This is confirmed by the fact that the whole range of load cycles considered in the experiments could be covered only for material E with an average error of 13%; errors for materials C, D and G ranged between 12% and 22% for the first 300,000/400,000 cycles performed in the tests; Weibull distribution could not fit experimental data for materials F and U. The data plotted in the figure were instead best fitted by negative exponential (materials C and D), power (materials E and F) and inverse logarithmic (materials G and U) functions; the corresponding correlation coefficients R^2 ranged between 0.908 and 0.982. The non-Weibull best fit for material E is included in the plot: it yields $R^2 = 0.908$ and practically coincides with the corresponding Weibull fit.

5. DISCUSSION OF THE RESULTS

5.1 Significance of experimental tests

The purpose of this work was to simulate as close as possible the operating conditions that occur in an actual railroad wheel. The initial damage of an actual wheel is shown in Figure 1 and is a typical crack observed in the wheel tread. Figure 12 shows a crack formed in the simulated wheel after $8 \cdot 10^5$ rolling cycles. Figure 13 shows a representation in μm of the two crack profiles together with a displaced version of the crack of the simulated wheel to adjust for the distance of the crack to the tread surface. The paths of the two cracks are very similar. It can be concluded

that the adopted similitude design approach reproducing the contact area in reduced scale, that is a scale reproduction of the actual wheel contact ellipse and yields the same stress level, has worked out well. Consequently, the wheel model gives a realistic picture of the processes occurred in the field. However, some differences should be pointed out.

The surface crack growth in the small wheel is limited to approximately the width of the track. In the initial conditions, the minor axis of the contact ellipse is 460.1 μm. The maximum crack length observed in a microscopic view was on average 270 μm, that is of the order of magnitude of the crack width. The total length of the crack represented in Figure 13 is 217.5 μm. Consequently, one can assume that the deepest crack observed experimentally is a curved surface in space with develops on the surface and in depth almost by the same extent. In the actual wheel, the minor axis of the contact ellipse is 5.659 mm and the surface crack length observed covers the entire region where the contact between the wheel and the rail takes place. It should be remembered that the contact regions in actual wheels move thus covering a wider area than the contact area. Also the tangential load is not applied all the time, but takes place during braking and curving. The profile of Figure 1 is typical of the crack depth observed in the actual railroad wheel; it has practically in depth the same geometry and the same length than the simulated wheel but corresponds to three orders of magnitude larger number of cycles. Roughly it can be said that the life of the model wheel of $8 \cdot 10^5$ corresponds to $1.1 \cdot 10^8$ cycles of the actual wheel. Furthermore, the crack length observed in the actual wheels on the surface is much longer than the contact area. The crack ceases to propagate in depth after a certain number of cycles but can still propagate on the surface.

Of course, this is one single set of observations but it gives an idea of the correspondence between an actual wheel and a simulated wheel in the laboratory. The laboratory test can be considered as an accelerated test but still provides good clues on the mechanism of crack formation and the response of different materials and thermal treatments to the service conditions.

5.2 Damage mechanism

In order to understand the process of wheel damage, first it is necessary to analyze the actual observed phenomena. Figure 14 shows a schematic view of the testing set up. A tangential force is applied to the model wheel in the direction of rotation and this force causes plastic flow in the direction of the applied force.

Figures 15 and 16 show cross sections taken parallel to the track. From these micrographs of the metal follows that very large plastic deformations take place up to about 200 μm in depth.

The magnitude of the deformations can be estimated from the changes in dimensions of the steel grains and of the texture of the surface. In a railroad wheel the contact stress distribution is very complex and depends heavily on the friction forces between the two contacting surfaces and on the applied tangential forces. There is an adhesion region and a slipping region: the former corresponds to the front part of the contact area. The size and position of the adhesion zone depend on the normal and tangential forces applied to the wheel. It is in this adhesion zone where the larger plastic deformations take place.

Generally speaking, the basic issue in understanding the actual physics of the contact is to identify the adhesion region and the slipping region. These two regions always exist if the contact has friction. In the adhesion region the two materials deform together by molecular adhesion. In the slipping region the two materials have relative displacements that in the railway nomenclature are called creep. If we have a symmetric surface, separation between the two areas will have the same symmetry. For example, if the contact area is a circle (such as in the case of the contact involving a spherical surface), the separation will be a circle. Similarly, if the contact area is an ellipse (such as in the case of the contact involving a cylindrical surface), the limit between the adhesion and slipping regions will be an ellipse.

A previous study carried out by the first author considered the case of a semi-spherical ball of highly polished steel in contact with a simulated infinite plane made of plexiglass [25,26]. The moiré technique [25] was used for analyzing contact stresses developed under static normal load and friction. The experimental set up utilized in those experiments is shown in Figure 17-a. The plane containing the grating is the plane of symmetry of the plexiglass prism. The contact region in this case is a circle; because of symmetry, the 3-D distribution of stresses can be studied in 2-D, in the symmetry plane where the XY reference system is set. As expected, friction changed distributions of normal/shear strains with respect to the classical Hertz's solution. Figures 17b-d illustrate the presence of the two regions: the region of low shear corresponds to the adhesion area while the pic area corresponds to the slipping region.

As the contact becomes dynamic the symmetry of adhesion region and slipping region disappears. This is confirmed also by a previous study carried out by the first author [27] where residual strains caused by rail-wheel contact were measured with the moiré method. A model wheel (the same as that used in the present study but with a flat surface rail of curvature radius equal to infinity) was applied to a rail where a cross grating was engraved. The wheel was subjected to a normal force and a tangential force. The grating was deformed because of the rail-wheel contact and analyzed using the moiré method. The lines of principal plastic strains corresponding to contact with normal force and a torque were obtained from the study of the

moiré pattern and correspond to the residual plastic deformations left by the effect of the rolling contact in the rail. It can be seen that the front part of the wheels experiences very high strains as indicated by the residual strains left by the applied forces (see Figure 18-a). These strains are in the direction of the rolling. In the transversal direction also there are very large permanent strains (see Figure 18-b). Although it is an idealization of the process of contact it provides useful information concerning the size of the adhesion region and the slipping zone.

Figure 19 gives another clue on the development of the rolling contact process. It comes from experimental measurements made by impending rolling [28,29], corresponding to a cylindrical wheel [30]. Moiré techniques were used for measuring displacements and strains caused by contact. In the figure, actual measured strains have been scaled to make the visual comparison clearer. The values given in [28,29] correspond to the center line of the contact area while the values measured in [30] correspond the centerline of the contact ellipse. Since dimensions of the major axis of contact ellipse depend on the load and materials, the position of points is normalized by making the half axis equal 1.

Figure 19 is the equivalent of plotting the strain ε_{xx} of Fig. 17: it shows that in rolling contact, the attack zone hosts high tensile stresses that are the source of the bulk cracks. It can be seen that there is a qualitative agreement between the strain distributions of the cylindrical roller [28,29] and the residual strains measured for the cylindrical wheel [30], in spite of the difference in materials (the cylindrical roller was made of plexiglass and the supporting plane was made of urethane rubber). In the contact region there is an adhesion zone, which in Figure 17-b corresponds to the region limited by the points where strain ε_{xx} becomes equal to zero (and then becomes positive) and the slip region, which is the rest of the contact area. Due to the symmetry of the problem in this case the adhesion and the slip regions are concentric.

The effect of the tangential force is to displace the adhesion zone where longitudinal strain became positive to the front of contact area (“attack region”) as it is shown in Figure 19 (according to the sketch of Figure 18, the attack region corresponds is the right edge of Figure 19). As the wheel rolls subjected to tangential force, an element of volume enters the contact area and experiences large contact forces that produce high tensile stresses and low to moderate normal forces. Then, it experiences increasing compressive stresses that go down as the element leaves the contact area. From the micrographs one can see that the cracks penetrate a region that is not isotropic but has a layered structure and is heavily damaged and slowly changes with the depth.

Another clue of the process of crack formation and growth can be obtained from Figure 20 [31]. This photoelastic pattern was obtained for a two dimensional plate representing an infinite

elastic half-plane loaded by a distributed force in a region of the boundary. The isochromatics are lines of equal shear stress. In Figure 20, we have added the crack profile plotted in Figure 13 matching the scale of the figure. It can be seen that the cracks approximately follow lines of maximum shear stress produced by the vertical load. However, there is also a horizontal load that modifies the contact zone as well as stress and strain distributions.

It should be noted that Figure 20 is quite relevant because there are several damage mechanisms activated by the rolling contact of two surfaces. There is a surface damage caused by the presence of roughness that through high cycle fatigue leads to the scaling separation of material (see Figure 22). A separate mechanism of damage is related to fatigue, caused by the bulk stress field leading to the formation of the cracks shown in Figures 1 and 12. This process is a classical fatigue crack propagation under a 3-D stress state. A recent experimental verification in this regard is presented in [32]. The fracture takes place along the isostatics of the stress field that are lines of maximum damage. In the present case, the lines of maximum damage are the lines of maximum shear. This explains the similitude of shape between the observed shear strains in the photoelastic pattern and the crack trajectory observed in the present experiments. The shear stresses correspond to contact stresses with friction and are shown as additional information to help the reader to visualize the stress field that prevails in the contact problem.

If one wants to describe crack mechanics, the anisotropy and the damage process cannot be neglected. It has been remarked that crack approximately follows the regions of constant shear stress. The cracks on the surface are statistically perpendicular to the track and, as said before, do not grow on the surface much larger than in depth: therefore, both surface and depth crack lengths are about the same. The average speed of propagation can be easily computed: surface crack grows about 200 μm in $7 \cdot 10^7$ cycles, this gives a velocity of crack growth per cycle da/dN=0.29 nm/cycle, or roughly 3 atomic radiuses per cycle. Consequently, the crack growth rate is of the order of $3 \cdot 10^{-10}$ m/cycle. There are micro-structurally short cracks of the order at maximum of 200 μm: hence, cracks are of the dimensions of the grain sizes. Most theories on crack growth are based on the continuum mechanics approach, for example the Paris' law

$$\frac{da}{dN} = C \, \Delta k_{eff}{}^{m} \tag{6}$$

However, the material does not behave any longer as an isotropic and homogeneous material at the scales corresponding to the 200 μm cracks. The crack growth is determined by the micro-structural features of the material. The speed of propagation can be quite irregular; the crack can grow very quickly in highly damaged areas and be arrested by crystal barriers in other

regions. It should be mentioned that in the present case there were no individual cracks but there are ensemble averages of thousands of cracks. In this sense, one can apply Paris' law in its generalized form shown in Eq. (6). According to the calculated average speed of propagation, we are, in the case of steels, very near the ΔK_{th} (threshold ΔK) which is a function of the ratio of minimum to maximum stresses applied (generally referred to in the literature as R) and on the presence of structural features that tend to block the crack propagation and are characterized by some length parameter (characteristic of the material structure), and also depends on environmental variables.

There are in the literature many expressions that were derived to represent the threshold behavior and that can be fitted to a particular set of data. One can take the nominal Δk value

$$\Delta k = Y \Delta\sigma \sqrt{\pi a} \tag{7}$$

where Y is the geometric factor, $\Delta\sigma$ is the stress increment applied, a is the crack length. Although the crack has a three-dimensional nature and on the surface the square root singularity is not valid, experimental investigations (based on holographic interferometry), supporting the development of series solutions to the stresses and displacements around the crack tip then utilized to find the stress-intensity factor along the flaw border [33], show that stress intensity factor values are reasonably well described by Eq. (7).

There is a very important aspect to be considered which confirms that one should be very cautious at using the idea of plasticity when a dynamic phenomenon like fatigue is involved. Plasticity itself is a dynamic phenomenon that implies the motion of dislocations. This process implies the propagation of dislocations in waves, motion that is triggered by the loading process [34]. The material in the initial condition is elastic and as it is being loaded by the contact forces follows a stress-strain relation corresponding to a 3-D stress condition. Consequently, for a given level of load, dislocations are no longer stable and begin to propagate in a plastic wave that increases the damage of the material by coalescence of the dislocations within the volume. However, since at a certain instant of time the load is reduced because of the fatigue cycle the material returns to the elastic state. This cycle repeats itself until in the damage zone coalescence of dislocations creates an actual crack that ultimately will lead to the fracture if the void created is big enough to generate the instability of the whole structure. Although the process is very complex to model, it is possible on the basis of existing knowledge to make inferences in a statistical sense as it was done in the present study.

The experiments carried out in this study show that crack generation and propagation (in particular, ensemble average-crack density and average length of surface cracks and the

quantities derived from these parameters) follow a Weibull's type statistical distribution. Variations of the rate of change of number of cracks $\partial N_{CR}/\partial N$ and rate of change of average crack length $\partial L_A/\partial N$ with respect to the number of load cycles are plotted in Figure 21. Similar to the $\partial N_{CR}/\partial W$ and $\partial L_A/\partial W$ trends shown in Figures 10 and 11 (it be must recalled that wear increases linearly with cycles), negative exponential, inverse logarithmic and power function fittings are more accurate than the Weibull distribution: in fact, correlation coefficients R^2 ranged between 0.937 and 0.975 ($\partial N_{CR}/\partial N$) or between 0.945 and 0.982 while Weibull fittings of $\partial N_{CR}/\partial N$ and $\partial L_A/\partial N$, respectively, resulted in average errors always greater than about 14% and 12% (for material E; furthermore, Weibull fit of $\partial L_A/\partial N$ practically coincides with the power function best fit). Interestingly, data relative to material E were always fitted by a power function with negative exponent values ranging between -0.823 and -0.775.

The local damage creates favorably oriented grains where the crack propagation can take place at higher speeds than those corresponding to the nominal stresses applied. As the crack penetrates in the interior of material the surface structure is less damaged. At the same time, through-depth stresses are reduced and hence the crack speed will slow down until the crack comes to rest. Considering the speed of crack length generation depicted in Figure 21-b, it is possible to see that speed goes down as the number of cycles increases.

As far as it concerns the crack length density observed in the experiments, two processes of crack generation must be highlighted. There are local contact stresses, generated by the irregular contact between the two surfaces, and global stresses. The local contact stresses cause the wear while the global stresses generate the cracks that penetrate in depth. The wear leads to the formation of debris under the form of metal flakes. This type of debris is the same in the experimental model and in an actual railroad wheel as shown in Figure 22.

The plots of the derivatives of the number of cracks and length with respect to the number of cycles, given in Figure 21, show that both the number of cracks generated per unit area and their lengths come to a steady state or a sort of a stable process. Interaction between cracks will cause shielding of the cracks. The surface cracks generated will balance with the crack removed by the wear. The longer cracks that correspond to the fracture penetrating in the wheel's ream will also slow down to a halt defining a sort of maximum density of crack formation. The situation will change if a liquid is present in the wheel that penetrates in certain cracks and finds some inner defects that will propagate cracks further inside the wheel. This situation may be helped by unusual overloads and steep braking.

6. CONCLUDING REMARKS

An experimental approach to evaluate rolling contact fatigue of six different materials employed in rail wheel constructions was developed in this study. Laboratory conditions were successfully scaled to actual railroad conditions and crack formation/propagation mechanisms were analyzed on a statistical basis. The fatigue contact problem is very complex because of the large amount of variables that need to be considered to perform the corresponding analysis. Purely numerical or analytical studies will not be correct if they are based on the usual assumptions of material homogeneity and isotropy on which continuum mechanics approach relies. However, actual observed phenomena on the basis of a statistical analysis can provide clues on the critical variables governing the damage evolution of surface fatigue.

A very important conclusion that can be drawn from this work is that for multi-axial fatigue cases like the one considered in this study the idea of damage is fundamental. The introduction of empirical quantities based on the classical continuum mechanics arguments cannot lead to adequate representation of the studied problem. One has to experimentally observe the actual events, relate them to basic mechanics formulations and then create models that must take into consideration the structural changes taking place in the material which in turn are dependent on geometrical and loading variables as well as on material properties. A material has a memory that keeps record of the previous stress/strain history and the crack propagation will be depending on such history. For example, in the particular case analyzed in the study we can see that crack trajectories can be modeled by lines of maximum shear. However, it could be not correct to state that the crack in the wheel is a mode II crack type. In fact, the possibility that all modes of crack propagation will be activated has to be addressed, since the crack trajectories will be affected by the previous stress/strain histories.

REFERENCES

[1] Lundén R, Paulsson B. Wheel–Rail Interface Handbook. Elsevier; 2009. doi:10.1533/9781845696788.1.3.

[2] Lundberg G, Palmgren A. Dynamic Capacity of Rolling Bearings. Generalstabens litografiska anstalts förlag; 1947.

[3] Kondo Yoroizaka, K., Sato, Y. K. Cause, increase, diagnosis, countermeasures and elimination of Shinkansen shelling. Wear 1996;191:199–203. doi:10.1016/0043-1648(95)06727-2.

[4] Cannon DF, Pradier H. Rail rolling contact fatigue Research by the European Rail Research Institute. Wear 1996;191:1–13. doi:10.1016/0043-1648(95)06650-0.

[5] Sadeghi F, Jalalahmadi B, Slack TS, Raje N, Arakere NK. A Review of Rolling Contact Fatigue. J Tribol 2009;131:041403 1–15. doi:10.1115/1.3209132.

[6] Jin X, Xiao X, Wen Z, Guo J, Zhu M. An investigation into the effect of train curving on wear and contact stresses of wheel and rail. Tribol Int 2009;42:475–90. doi:10.1016/j.triboint.2008.08.004.

[7] Zhong W, Hu JJ, Li ZB, Liu QY, Zhou ZR. A study of rolling contact fatigue crack growth in U75V and U71Mn rails. Wear 2011;271:388–92. doi:10.1016/j.wear.2010.10.071.

[8] Brouzoulis Ekh, M. J. Crack propagation in rails under rolling contact fatigue loading conditions based on material forces. Int J Fatigue 2012;45:98–105. doi:10.1016/j.ijfatigue.2012.06.002.

[9] Wang G, Qu S, Lai F, Li X, Fu Z, Yue W. Rolling contact fatigue and wear properties of 0.1C–3Cr–2W–V nitrided steel. Int J Fatigue 2015;77:105–14. doi:10.1016/j.ijfatigue.2015.02.019.

[10] Bevan A, Molyneux-Berry P, Eickhoff B, Burstow M. Development and validation of a wheel wear and rolling contact fatigue damage model. Wear 2013;307:100–11. doi:10.1016/j.wear.2013.08.004.

[11] He CG, Huang YB, Ma L, Guo J, Wang WJ, Liu QY, et al. Experimental investigation on the effect of tangential force on wear and rolling contact fatigue behaviors of wheel material. Tribol Int 2015;92:307–16. doi:10.1016/j.triboint.2015.07.012.

[12] Seo J-W, Jun H-K, Kwon S-J, Lee D-H. Rolling contact fatigue and wear of two different rail steels under rolling–sliding contact. Int J Fatigue 2016;83:184–94. doi:10.1016/j.ijfatigue.2015.10.012.

[13] Donzella G, Faccoli M, Ghidini A, Mazzù A, Roberti R. The competitive role of wear and RCF in a rail steel. Eng. Fract. Mech. 2005;72:287–308. doi:10.1016/j.engfracmech.2004.04.011.

[14] Wang WJ, Guo J, Liu QY, Zhu MH, Zhou ZR. Study on relationship between oblique fatigue crack and rail wear in curve track and prevention. Wear 2009;267:540–44. doi:10.1016/j.wear.2008.12.100.

[15] Ramalho A. Wear modelling in rail–wheel contact. Wear 2015;330-331:524–32. doi:10.1016/j.wear.2015.01.067.

[16] Mazzù A, Solazzi L, Lancini M, Petrogalli C, Ghidini A, Faccoli M. An experimental procedure for surface damage assessment in railway wheel and rail steels. Wear 2015;342-343:22–32. doi:10.1016/j.wear.2015.08.006.

[17] Mazzù A, Petrogalli C, Faccoli M. An integrated model for competitive damage mechanisms assessment in railway wheel steels. Wear 2015;322-323:181–91. doi:10.1016/j.wear.2014.11.013.

[18] Mazzù A. A numerical approach to subsurface crack propagation assessment in rolling contact. Fatigue Fract Eng Mater Struct 2013;36:548–64. doi:10.1111/ffe.12024.

[19] Donzella G, Mazzù A, Petrogalli C. Failure assessment of subsurface rolling contact fatigue in surface hardened components. Eng Fract Mech 2013;103:26–38. doi:10.1016/j.engfracmech.2012.05.009.

[20] Donzella G, Mazzù A. Extension to finite life of a failure assessment diagram for contact fatigue loading. Int J Fatigue 2012;44:217–24. doi:10.1016/j.ijfatigue.2012.04.014.

[21] Kalker JJ. Wheel-rail rolling contact theory. Wear 1991;144:243–61. doi:10.1016/0043-1648(91)90018-P.

[22] Wang P. Design of High-Speed Railway Turnouts. 1st ed. Academic Press; 2015.

[23] Makino T, Neishi Y, Shiozawa D, Fukuda Y, Kajiwara K, Nakai Y. Evaluation of rolling contact fatigue crack path in high strength steel with artificial defects. Int J Fatigue 2014;68:168–77. doi:10.1016/j.ijfatigue.2014.05.006.

[24] Sciammarella CA, Kumar S, Nailescu L, Seth BB. Similitude Law for the Creep-Adhesion Function in Dry Contact. J Eng Ind 1979;101:278. doi:10.1115/1.3439508.

[25] Sciammarella CA, Sciammarella FM. Experimental Mechanics of Solids, Wiley, Chichester (UK), 2012.

[26] Sciammarella CA, Bath G. Computer assisted moiré method, In: Proc. Euromechanics Colloquium No.256 on Non-destructive 3-D stress analysis, Tallin (Estonia), 1989.

[27] Sciammarella CA. *Friction Creep and Wear Studies Between Steel Wheels and Rails*. U.S. Department of Transportation, Federal Administration Office of Development and Reseach, Report N FRA-OR and D-76-271, July 1976.

[28] Bremond CH. Resolution de problems de contact elastique plan avec frottement a partir de donnees experimentales. Ph.D. Thesis, Claude Bernard University, Lyon, France, 1976.

[29] Bremond CH, Durelli JA. Experimental analysis of displacements and shears at surfaces of contact. Exp. Mech. 1981; 21:105-110.

[30] Sciammarella CA, Albertazzi A. Measurement of residual stresses by the moire method. SEM Conf. Exp. Mech., Albuquerque (NM) USA: 1990, p. 419–26.

[31] Frocht MM. Photoelasticity: Volume 2. New York, USA: John Wiley and Sons; 1948.

[32] Sciammarella CA, Casavola C, Lamberti L, Pappalettere C. Investigation on fracture behaviour of turbine blades under self-exciting modes. Strain 2011; 47-S1: e113-e129.

[33] Dally JW, Sciammarella CA, Shareef I. Extraction of Stress-Intensity Factor from In-Plane Displacements Measured by Holographic Interferometry. Surface-Crack Growth Model Exp Struct 1990;1060:130–41.

[34] Sciammarella CA, Lamberti L, Merging experimental evidence and Molecular Dynamics theory to develop efficient models of solids fracture. Proceedings of the 2016 SEM Conference on Experimental and Applied Mechanics, Orlando (FL), USA, 2016.